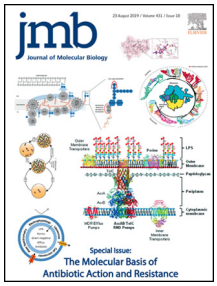

Novel and Improved Crystal Structures of *H. influenzae*, *E. coli* and *P. aeruginosa* Penicillin-Binding Protein 3 (PBP3) and *N. gonorrhoeae* PBP2: Toward a Better Understanding of β-Lactam Target-Mediated Resistance

Dom Bellini [1,†], Lizbé Koekemoer [2,3,†], Hector Newman [1,†] and Christopher G. Dowson [1]

*1 - **School of Life Sciences,** University of Warwick, Coventry, CV47AL, UK*
*2 - **H3D,** Institute of Infectious Disease and Molecular Medicine, University of Cape Town, Rondebosch 7700, South Africa*
*3 - **Structural Genomics Consortium,** University of Oxford, Roosevelt Drive, Oxford OX3 7DQ, UK*

Correspondence to Christopher G. Dowson: *c.g.dowson@warwick.ac.uk*
https://doi.org/10.1016/j.jmb.2019.07.010

Abstract

Even with the emergence of antibiotic resistance, penicillin and the wider family of β-lactams have remained the single most important family of antibiotics. The periplasmic/extra-cytoplasmic targets of penicillin are a family of enzymes with a highly conserved catalytic activity involved in the final stage of bacterial cell wall (peptidoglycan) biosynthesis. Named after their ability to bind penicillin, rather than their catalytic activity, these key targets are called penicillin-binding proteins (PBPs). Resistance is predominantly mediated by reducing the target drug concentration *via* β-lactamases; however, naturally transformable bacteria have also acquired target-mediated resistance by inter-species recombination. Here we focus on structural based interpretations of amino acid alterations associated with the emergence of resistance within clinical isolates and include new PBP3 structures along with new, and improved, PBP-β-lactam co-structures.
© 2019 Published by Elsevier Ltd.

Introduction

Penicillin and the wider family of β-lactams have remained the single most important class of antibiotics since their introduction in the early 1940s. The periplasmic/extra-cytoplasmic targets of penicillin are a family of enzymes with a highly conserved catalytic activity involved in the final stage of bacterial cell wall biosynthesis: cross-linking of the structural polymer peptidoglycan (PG). These enzymes are named penicillin-binding proteins (PBPs), based on their ability to bind penicillin rather than describing their catalytic activity [1–3]. Furthermore, PBPs have confusing nomenclatures based upon their SDS-PAGE gel migration patterns and are divided into high-molecular-mass (HMM) and low-molecular-mass (LMM) PBPs. Generally, gram-positive and -negative bacteria have multiple HMM and LMM PBPs. HMM PBPs are involved in the late stages of PG synthesis with class A HMM PBPs catalyzing both polymerization of the PG precursor-lipid II *via* transglycosylation and 4–3 crosslinking-transpeptidation, while class B HMM PBPs can only carry out transpeptidation. The equally essential class A and class B HMM PBPs have been linked to processes involved in cell elongation, shape determination and septation [1], and suppression of these PBPs variously causes cell lysis, cessation of cell division, filamentation and the formation of spherical cells [4]. Class C LMM PBPs catalyze carboxypeptidase and/or endopeptidase reactions [5,6] and are mainly involved in the maintenance, remodeling and recycling of PG [6].

Typically, *in vitro* deletion of all the LMM PBPs, although deleterious, is not fatal to the bacterium [6]. While all PBPs contain a penicillin-binding domain (PBD) HMM PBPs possess other domains, which vary significantly among the classes. The non-penicillin-binding domain (*n*-PBD) of the class A enzymes exhibits glycosyltransferase (GT) activity, while the corresponding *N*-terminal domain in the class B PBPs, although poorly characterized, is believed to serve as a stalk which allows the *C*-terminal TP domain to access PG [6]. Class B PBPs, for example, PBP 2× in gram-positives, can also contain *P*BD *a*nd *S*erine/*T*hreonine kinase *A*ssociated (PASTA) domains [7].

Despite the development of new classes of β-lactams since the advent of penicillin, resistance to these antibiotics remains a global problem [8]. The predominant resistance strategy against β-lactams is to reduce the drug concentration either by catalyzing their inactivation with β-lactamases [4,9–12], by increasing their efflux, or, in the case of gram-negative bacteria, by reducing permeation into the periplasm [13]. Furthermore, bacteria can respond to antibiotic treatment by developing target-based resistance; in the case of β-lactams, this is due to the evolution of so-called "low–affinity PBPs," which require elevated antibiotic concentrations to be inactivated, although the precise mechanisms for this phenotype are still poorly characterized. A structurally informed analysis of this PBP-mediated resistance through target mutations is the focus of this review. More specifically, we focus on an essential class B HMM PBP found across gram-negative bacteria that play a crucial role in cell division [14]. This PBP is typically identified by gel migration as PBP3 and encoded by the *ftsI* gene, with the exception in *Neisseria* spp. where it is referred to PBP2 and encoded by the *penA* gene.

These homologous PBPs represent individual key targets across gram-negative bacteria for β-lactam therapy and are often the primary PBP target with the lowest IC_{50} for a range of penicillins, cephalosporins, the monobactam aztreonam, and therefore a potential pinch point for the development of PBP-mediated resistance [15] [16]. β-Lactamase-negative, ampicillin-resistant (BLNAR) clinical isolates of *Neisseria meningitidis* and *Haemophilus influenzae*, exhibiting PBP-mediated resistance, with low affinity PBP2/PBP3s have been reported for many years [17,18]. Interestingly, both the *Neisseria* spp. and *H. influenzae* are naturally transformable and mosaic *ftsI* genes are found in clinical isolates that have arisen by interspecies recombination with commensal members from each genus *Neisseria flavescens* and *H. haemolyticus*, respectively [19,20]. Altered PBP mosaic blocks [21] can encode multiple amino acid alterations, some of which have been identified as being involved in resistance [22–24], while others may simply have "hitch-hiked" along with those residues offering the selective advantage of resistance or are yet to be determined, including potential compensatory alterations required for fitness. However, non-mosaic, presumably spontaneous, point mutations in PBP2/PBP3s have also been observed to generate resistance to both the penicillins and cephalosporins. To date, numerous papers have described the distributions of PBP2/PBP3 alterations from organisms including *Neisseria gonorrhoeae* [25], *H. influenzae* [26,27], *Pseudomonas aeruginosa* [28] and *Escherichia coli* [29], suggesting that this mechanism of PBP-mediated resistance is becoming more common. Despite all this available genetic information, there is little mechanistic understanding of how these point mutations lead to decreased β-lactams affinity by the PBP3s.

In an attempt to address this shortcoming, we present here a novel PBP3 TP domain crystal structure from the pathogen *H. influenzae*, as well as previously reported PBP3 structures with improved resolution from *E. coli*, *P. aeruginosa* and *N. gonorrhoeae*. We used these structures to map locations of known resistance mutations on to the TP structural domains of PBP3 for each of these species. We hope that our structural approach will lead to further insight into the mechanism of action of these widely reported, but poorly understood, mutations.

Results

Crystal structures of various TP domains

The following crystal structures were obtained: (1) five isomorphous structures of *Pa*PBP3 lacking the transmembrane helix: three of wild type *Pa*PBP3* (apo, 1.2 Å, piperacillin-acylated, 1.59 Å and amoxicillin-acylated, 1.64 Å) and two of the mutant *Pa*PBP3*^{R504C} (apo, 2.2 Å, and piperacillin-acylated, 1.7 Å); (2) two isomorphous structures of *Ec*PBP3 TP domain: *Ec*TP3 (apo, 1.95 Å; piperacillin-acylated, 1.75 Å); (3) TP domain from a clinical mutant of *Ng*PBP2: *Ng*TP2$^{HR-6140}$ (apo, 1.43 Å); and (4) *Hi*PBP3 TP domain containing four artificial mutations to aid crystallization: *Hi*TP3^{FEKQ} (apo, 2.44 Å). All protein–ligand complexes were derived by soaking a native crystal in mother liquor containing the ligand. The initial structures were determined using available PDB coordinates of *Pa*PBP3 (PDB code 3OC2) for *Pa*PBP3*, *E. coli* lower-resolution (2.5 Å) PBP3* (PDB code 4BJP) for *Ec*TP3 and *Hi*TP3^{FEKQ}, and *N. gonorrhoeae* lower-resolution (2.2 Å) PBP2 TP domain (PDB code 4U3T) for *Ng*TP2$^{HR-6140}$ as molecular replacement models. Crystallographic statistics are shown in Table SI_1.

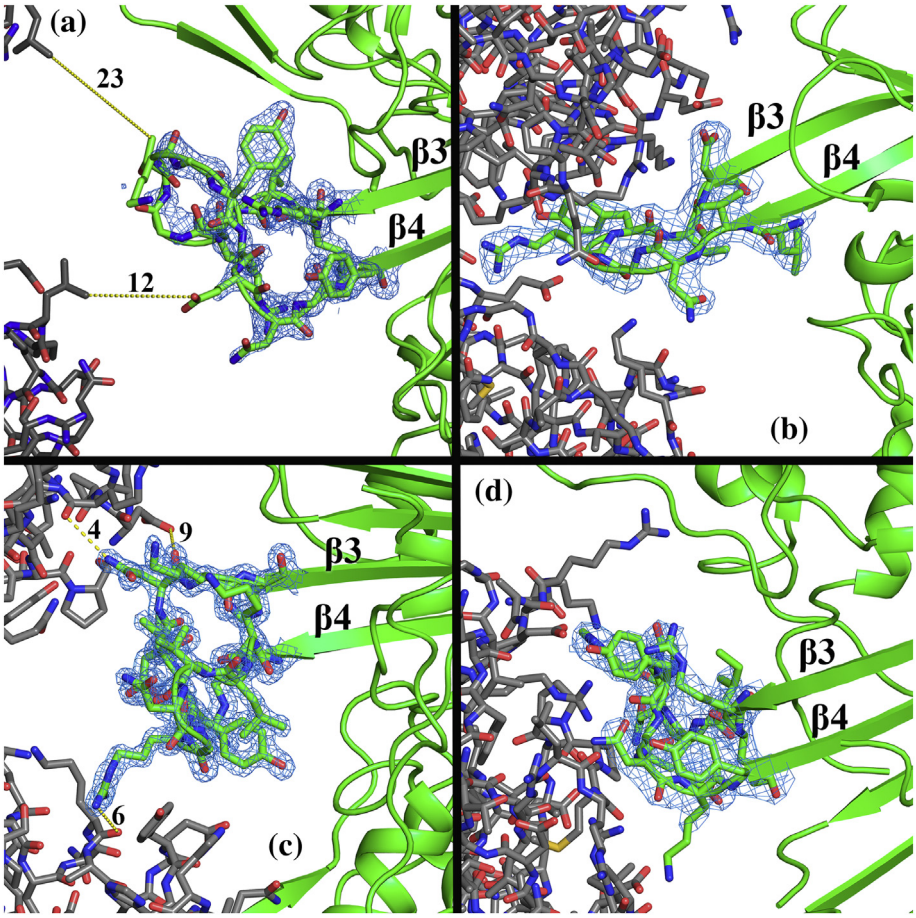

Fig. 1. Comparison of crystallization contacts in the β3–β4 loop of different PBP3 structures. Panels a, b, c and d show piperacillin-acylated *Pa*PBP3*, *Ng*TP2$^{t3–6140}$, *Ng*TP2$^{HR-6140}$ and *Hi*TP3^{FEKQ} structures, respectively; the electron density is at a contour level of 1.3, 1.7, 1.5 and 1.4 σ, respectively. Crystallographic symmetry-related molecules are colored in gray. Intermolecular interactions are indicated by yellow dash and the distances are shown in Å.

P. aeruginosa PBP3* structures

The apo structure of *Pa*PBP3*, including both *N*-terminal and *C*-terminal domains but lacking the transmembrane helix, reported in this work has a significantly higher resolution (1.2 Å *versus* 2.0 Å) compared to that previously deposited in the Protein Data Bank (PDB code 3OC2). Despite the higher resolution the β3–β4 loop, a hotspot for various PBP3-mediated resistance mutations (see later), is too flexible to be visible, which is similar to 3OC2. However, this loop is clearly visible in the amoxicillin- and piperacillin-acylated form of *Pa*PBP3*, as is usually the case in other *Pa*PBP3* structures with a bound β-lactam possessing a bulky R1 chain (Fig SI_1). Interestingly, the β3–β4 loop in PaPBP3* structures is not engaged in any crystallographic contacts (Fig. 1a). The amoxicillin-acylated *Pa*PBP3* structure is the latest of several *Pa*PBP3* structures in complex with various β-lactams now available in the PDB, whereas a piperacillin-acylated PaPBP3* structure was already available (PDB code 4KQO), although at lower resolution (2.3 rather than 1.7 Å). Superposition of the structures of wild type *Pa*PBP3* and mutant *Pa*PBP3*^{R504C} did not show any difference when comparing either the apo or piperacillin-acylated pair (RMSD of 0.4 and 0.3 Å, respectively). Similarly to wild-type PaPBP3* structures, the β3–β4 loop (naming convention from Pares *et al.* [40]) was also only visible in the β-lactam-acylated form of mutant *Pa*PBP3*^{R504C} and not in the apo structure. It should be noted that in comparing the acylated-forms, the β3–β4 loop is found to have identical conformations despite the presence of the ^{Pa}R504C resistance-associated mutation at the beginning of strand β4 (Fig. 2a). Interestingly, although PaPBP3* and *Pa*PBP3*^{R504C} structures are perfectly superposable and the R504 residue neither takes part in catalysis nor appears to interact directly with the inhibitor, nevertheless, a decrease in bocillin acylation rate *in vitro* was clearly observed

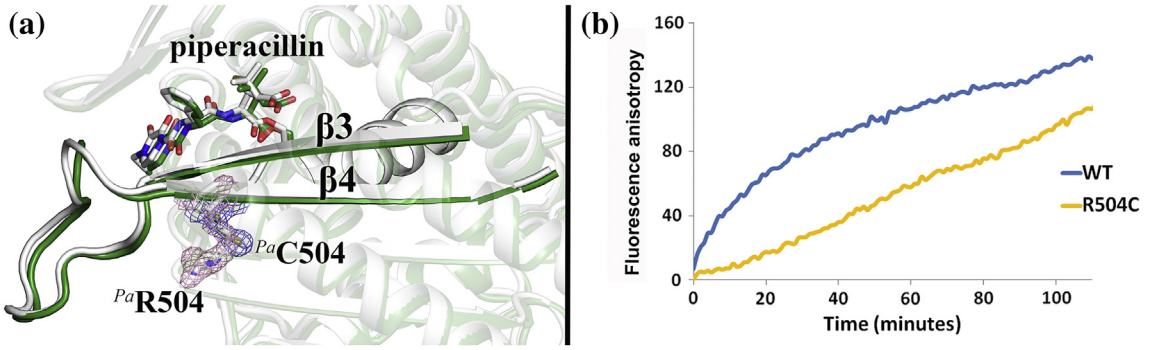

Fig. 2. Superposition of wild type (white) and ^{Pa}R504C mutant (green) of piperacillin-acylated *Pa*PBP3* structures. (a) The β3–β4 loop is highlighted and the mutation is confirmed by the electron densities at contour levels of 1.8 σ (colored pink for wild type and blue for ^{Pa}R504C mutant). (b) Results from *in vitro* bocillin fluorescence anisotropy assay of wild type and ^{Pa}R504C mutant *Pa*PBP3* proteins showing differences in acylation/deacylation rates.

in the case of the *Pa*PBP3^{R504C} mutant protein (Fig. 2b).

N. gonorrhoeae PBP2 TP domain structure

*Ng*TP2$^{HR\text{-}6140}$, the *N. gonorrhoeae* PBP2 structure truncated to the TP domain only, presented here was isolated from FA6140, a penicillin-resistant, non-penicillinase-producing strain first identified in 1983 [41] (Table 1). Although the crystal structure of this clinical mutant has been reported previously (PDB code 4U3T) [30], the structure reported in this work was solved at a significant higher resolution (1.4 rather than 2.2 Å) and with different conformations for two important loops: β2c–β2d and β3–β4. A number of *Ng*PBP2 mutant structures, all at 2.4 Å resolutions, are available in the literature for comparison with *Ng*TP2$^{HR\text{-}6140}$ (Table 1).

The FA6140 strain expresses a PBP2 with an aspartate insertion after D346, named D346a, with additional mutations at P551S + F504L + A510V + A516G. Prior to the first crystal structure by Fedarovich *et al.* [30], this aspartate insertion had been reported as D345a due to the lack of structural data. We use the notation D346a for consistency [30].

Comparing the structures containing the D346a insertion (*Ng*TP2$^{HR\text{-}6140}$ and *Ng*TP2$^{t3\text{–}6140}$) (Table 1) with the wild-type structure *Ng*PBP2*^{FA19} [31] indicates the potential dynamics introduced by this mutation into the β2c–β2d loop. While the three structures align well locally, with good agreement prior to R345 and after P352, the intervening residues appear to be able to follow two distinct pathways (Fig. 3a). In *Ng*TP2$^{t3\text{–}6140}$, the D346a insertion introduces a small "kink" in the loop, with T347 slightly displaced in a direction away from the active site. The loop realigns with that of the wild type by H348. In contrast the structure of *Ng*TP2$^{HR\text{-}6140}$ exhibits a much larger conformational change, with greatest displacements for T347 and V349, which have moved by 3.8 and 3.9 Å, respectively (displacements of Cα, relative to their positions in *Ng*PBP2*^{FA19}), and a rotation of Y350 away from the loop. Moreover, H348 is rotated almost 180° and displaced by 3.7 Å, which leads to the aromatic group occupying a space vacated by Y350. Interestingly, structures of *Ng*PBP2*^{6140CT} and *Ng*PBP2*^{A501T} (Table 1), which only have mutations in the *C*-terminal region of the TP domain, have the same β2c–β2d loop positioning as the wild-type structure *Ng*PBP2*^{FA19}, indicating that mutations to this region do not affect the position of the loop. Despite the difference in resolution between structures of *Ng*TP2$^{t3\text{–}6140}$ (2.2 Å) and *Ng*TP2$^{HR\text{-}6140}$ (1.4 Å), the density of the β2c–β2d loop is well defined in both cases (Fig. 3b and c), suggesting that loop displacement may be related to different crystal contacts and/or crystallization conditions such as pH (7.8 for *Ng*TP2$^{t3\text{–}6140}$ and 6.5 for *Ng*TP2$^{HR\text{-}6140}$).

The *Ng*TP2$^{HR\text{-}6140}$ structure showed electron density for the β3–β4 loop in both molecules in the asymmetric unit, unlike *Ng*TP2$^{t3\text{–}6140}$ where this loop is only visible in molecule A. Superposing molecule B of *Ng*TP2$^{HR\text{-}6140}$ to molecule A of *Ng*TP2$^{t3\text{–}6140}$ shows significant conformational change in the β3–β4 loop, which in *Ng*TP2$^{HR\text{-}6140}$ follows a similar path to that observed in the structure of *Ng*PBP2*^{A501T} (Fig. SI_2). This observation is important as Tomberg *et al.* [32] at the time concluded that the alternative conformation of the loop in *Ng*PBP2*^{A501T} (in comparison to wild type *Ng*PBP2*^{FA19}) was a result of the ^{Ng}A501T mutation in *Ng*PBP2*^{A501T}. However, since this mutation is absent in *Ng*TP2$^{HR\text{-}6140}$, it appears unlikely that this is the cause of the conformational change in the β3–β4 loop (Fig. SI_2). Fedarovich *et al.* [30] cautioned that interpretation of the conformations of the β3–β4 loop is challenging as it may be affected by artificial crystal packing interactions and high flexibility. A disordered β3–β4 loop could not be fitted in the wild-type structure of *Ng*PBP2* and was only fitted in one of the two molecules (molecule A) in the lower-resolution structure of *Ng*TP2$^{t3\text{–}6140}$. More importantly, the visible β3–β4 loop in *Ng*TP2$^{t3\text{–}6140}$ is

Table 1. Crystal structures of NgPBP2 mutants available in the PDB

	PDB Code	Mutations	Resolution (Å)	Publication
NgTP2$^{HR-6140}$	6HZJ	P551S + F504L + A510V + A516G + D346a	1.4	This publication
NgTP2$^{t3-6140}$	4U3T	P551S + F504L + A510V + A516G + D346a	2.2	[30]
NgPBP2*^{FA19}	3EQU	Wild type (strain FA19)	2.4	[31]
NgPBP2*^{6140CT}	3EQV	P551S + F504L + A510V + A516G	2.4	[31]
NgPBP2*^{A501T}	5KSH	P551S + F504L + A510V + A516G + A501T	2.4	[32]

The asterisk indicates that the transmembrane helix is missing in the construct.

constrained by various crystallographic contacts (PDB code 4U3T) [30] (Fig. 1b), whereas in *Ng*TP2$^{HR-6140}$ is not engaged in strong crystallographic contacts (Fig. 1c). This observation suggests that the structure of *Ng*TP2$^{HR-6140}$ could be exploited to study mutation-dependent conformational changes of the β3–β4 loop (see Discussion).

H. influenzae PBP3 TP domain structure

A construct of a modified TP domain from *H. influenzae* PBP3 (*Hi*TP3^{FEKQ}) was utilized to obtain crystals of diffraction quality of about 2.4 Å. The structure revealed, as expected from sequence alignment, a high degree of similarity between *Hi*TP3^{FEKQ}, other TP domains available in the PDB and from this work. The largest noticeable difference between *Hi*TP3^{FEKQ} and *Ng*TP2$^{HR-6140}$/*Pa*PBP3* TP domain is that the α10–β3 loop is shorter by 3 or 4 residues (Fig. 4a and b). The missing part of the α10–β3 loop is a glycine-rich region present in the other PBP3s (Fig. 4b), suggesting a loss of flexibility in this region for *Hi*PBP3. No function has been ascribed to this loop, although its position, capping the likely acceptor site, in the catalytic pocket suggests an interaction role with either the natural substrates or other proteins, rather than directly with β-lactam antibiotics. However, target-mediated resistance mutations in this α10–β3 loop of *Hi*PBP3 have been reported (see later). The β3–β4 loop is a hotspot for resistance mutations in class B PBPs. The electron density of this loop is clearly visible in all four copies of apo *Hi*TP3^{FEKQ} in the asymmetric unit. Interestingly, in all four copies of *Hi*TP3^{FEKQ}, this β3–β4 loop, which possesses a high degree of flexibility in other PBP3 structures, is constrained by identical crystallographic contacts (Fig. 1d).

E. coli PBP3 TP domain structure

The modified TP domain from *E. coli* PBP3 (*Ec*TP3) was utilized to obtain crystals of about 1.9 and 1.7-Å resolution for the apo- and piperacillin-acylated forms, respectively. These data represent significant improvement on the apo structure of *E. coli* PBP3* (lacking the transmembrane helix) previously reported by Sauvage *et al.* [42] at 2.5 Å (PDB code 4BJP). However, superposition of structures for *Ec*TP3 and *Ec*PBP3* TP domain indicates that the tertiary structure of this domain is virtually identical in the two constructs (RMSD = 0.42 Å) (Fig. SI_3).

Comparison between the apo- and acylated enzyme of different PBP3 TP domains

To simplify the discussion about the 5 catalytic residues conserved across all serine-transpeptidases, carboxypeptidases and serine-β-lactamases [5], the

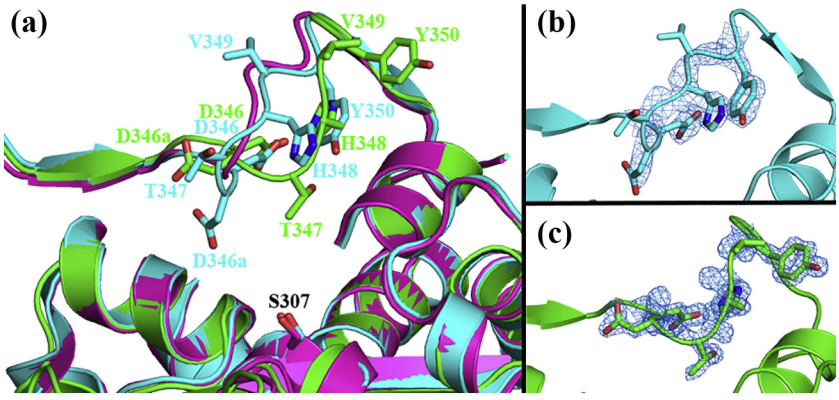

Fig. 3 Effects of the resistant-related inserted aspartate, ^{Ng}D346a, on the conformation of the β2c–β2d loop of different *N. gonorrhoeae* PBP2 structures. (a) Superposition of *N. gonorrhoeae* TP2 domains from structures of wild type NgPBP2*^{FA19} (3EQU, magenta), ^{Ng}D346a-containing lower resolution *Ng*TP2$^{t3–6140}$ (4U3T, cyan) and higher resolution *Ng*TP2$^{HR-6140}$ (this work, 6HZJ, green). Residues in the loops of mutants 4U3T and 6HZJ are represented in sticks, and the labels are colored relative to the corresponding structures. For clarity, wild-type loop (3EQU) is only shown in cartoon representation. The catalytic serine, S307, shown in stick as a reference point for the catalytic pocket, is labeled in black. Electron density of (b) 6HZJ and (c) 4U3T β2c–β2d loops are shown with contour levels of 1.7 and 1.5 σ, respectively.

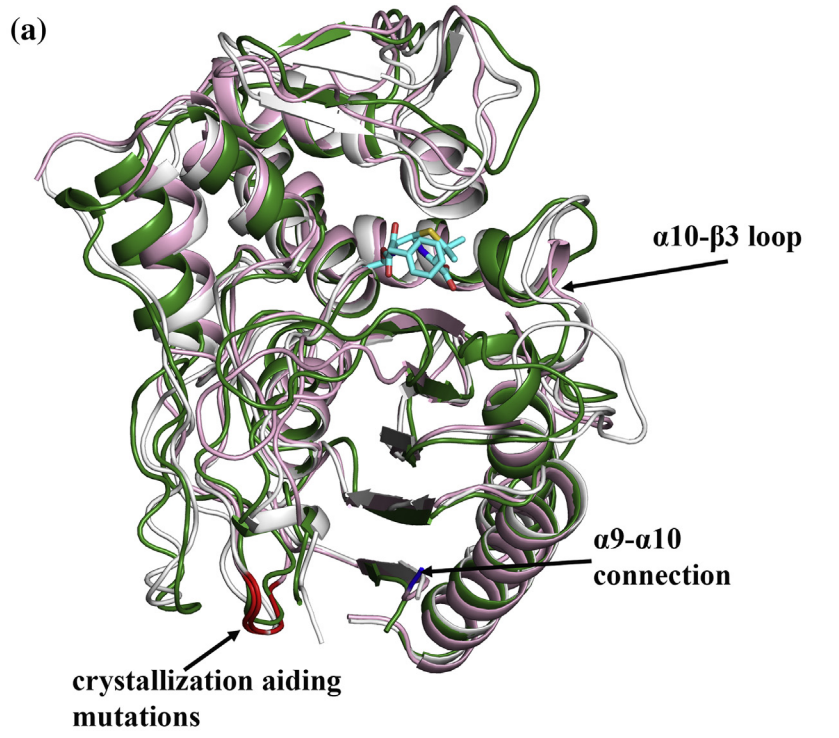

Fig. 4. Superposition of transpeptidase domains of structures *Hi*TP3^{FEKQ} (pink), *Ng*TP2$^{HR\text{-}6140}$ (green) and *Pa*PBP3* (white). (a) The α10–β3 loop is indicated. The crystallization-aiding mutations FEKQ are colored in red, and the glycine residue used to connect helix α9 to helix α10 after deletion of the predicted α9–α10 flexible loop is colored in blue. Penicillin G, represented in cyan stick, is superimposed in the catalytic pocket for reference. (b) Primary sequence alignment of various PBP3s showing the region around the α10–β3 loop; the K(S/T)G motif is shown in red color. *Paer* = *P. aeruginosa*, *Ecol* = *E. coli*, *Ngon* = *N. gonorrhoeae* and *Hinf* = *H. influenza*.

notation $\mathbf{S_1}$, $\mathbf{K_1}$, $\mathbf{S_2}$, **N** and $\mathbf{K_2}$ has been utilized. $\mathbf{S_1}$ and $\mathbf{K_1}$ are the serine and lysine from the active-site serine S*XXK motif, $\mathbf{S_2}$ and **N** are the serine and asparagine from the SXN motif, and $\mathbf{K_2}$ is the lysine from the K(T/S)GT motif. For example, in *E. coli* PBP3, these residues correspond to S307 ($\mathbf{S_1}$), K310 ($\mathbf{K_1}$), S359 ($\mathbf{S_2}$), N361 (**N**) and K494 ($\mathbf{K_2}$).[4] The *C*-terminal TP domain of PBP3 proteins (TP3) shows a highly conserved fold among all six structures presented in this work (Fig. SI_4). In all the apo-structures reported here the catalytic residues $\mathbf{K_1}$, **N** and $\mathbf{K_2}$ effectively show conserved rotamers, while $\mathbf{S_1}$ and $\mathbf{S_2}$ side chains can be found in different orientations (Fig. SI_5A). Particularly, the catalytic serine $\mathbf{S_1}$ is found in all three allowed rotamers among the various structures. The previously reported structure of *E. coli* PBP3 (PDB code 4BJP, cyan in Fig. 8A) and our *Ec*TP3 presented here (yellow in Fig. SI_5A) show $\mathbf{S_1}$ with different rotamers. This would suggest that differences in crystallization conditions and/or pH rather than mechanistic differences may play a role in this side-chain conformation. When comparing the acylation/deacylation rates of *Ec*TP3, *Hi*TP3^{FEKQ} and *Ng*TP2$^{HR\text{-}6140}$ with their corresponding full-length proteins, *Ec*PBP3*, *Hi*PBP3* and *Ng*PBP2* (lacking only the transmembrane helix) in enzymatic assays, similar rates were measured for the truncated and full-length enzymes (results not shown). Previous studies comparing *Ng*TP2 and *Ng*PBP2* with bocillin-FP assays also showed no difference in acylation rates [30].

Covalent attachment of β-lactams to PBPs is through the acylation of $\mathbf{S_1}$ and the drug-acylated $\mathbf{S_1}$ side chain is always found in a single conserved rotamer (Fig. SI_5B). Similarly, the D-Ala–D-Ala mimicking core present in all β-lactams adopts similar orientations in all different acylated-PBP3

structures presented in this work, as does conserved hydrogen-bonding interactions between the carbonyl and the amine of the R1 amide linkage with, respectively, the side-chain amine of **N** and main-chain carbonyl of a conserved threonine [last T from the K(T/S)G**T** motif], which are consistently maintained (Fig. SI_5B).

Although the substantial amount of available structural data indicates considerable rigid-body rotational freedom between the *N*- and *C*-terminal domains of the PBP3s, the overall conformation of the *C*-terminal catalytic domain remains largely unaltered upon covalent binding of inhibitors. This is seen by the superposition of various drug-bound TP domains of *Pa*PBP3* to that of the apo-enzyme which only results in RMSDs in the range of 0.4–0.5 Å. However, some significant local changes occur around the catalytic pocket upon covalent attachment of inhibitors compared to the apo-structure. The extent of these changes varies among the different species of PBP3s. In the case of *Pa*PBP3* strands β3 and β4, upon binding of amoxicillin, bend toward the acylated β-lactam around a hinge region itself located on these strands. This results in a movement of approximately 4 Å for the Cα atoms of the last and first ordered residues of the β3 and β4 strands (Fig. SI_6). This bending of β3 and β4 strands had previously been reported in *Pa*PBP3* upon binding of piperacillin [33]. Similar movements upon binding of β-lactams have also been reported in the corresponding strands of Gram positive PBPs, both class A and B [43,44]. Surprisingly, in the case of apo and acylated structures of *Ec*TP3 reported in this work, the β3 and β4 strands remain locked in one specific conformation, which is comparable to that of acylated *Pa*PBP3* (Fig. SI_6). The similarity discussed above between *Ec*TP3 and *Ec*PBP3* (Fig. SI_3 and Fig. SI_7) suggests that the lack of the *N*-terminal domain in the *Ec*TP3 construct does not appear to have any influence on the conformation of β3 and β4 strands in the apo form (there are no available structures for acylated *Ec*PBP3*). This supports the possibility that these strands in the catalytic pocket of *Ec*PBP3 possess a higher degree of rigidity than in other PBP3s where movements are observed between the apo and acylated forms of the protein.

Mapping of known β-lactam resistance-mediating mutations onto PBP3 structures

Mutational data for clinical isolates are readily available and several classification systems have been proposed based on different groupings [26,27,45,46]; however, this can make the interpretation and comparison of mutations between various PBP3 species challenging. In this review, a classification of mutation clusters is proposed based on secondary structure regions present across all PBP3s. The focus is primarily on five regions of mutation clusters for which data are readily available and have been consistently shown to affect resistance across different PBP3s: (1) the β2b–β2c–β2d region, (2) the α10–β3 region, (3) the β3–β4 region, (4) the α5–α6 region and (5) the β5–α11 region. In order to enhance readability, the species have been reported as superscript at the front of the mutation; for example, ^{Hi}R517H refers to a mutation in *H. influenzae*. The prefix *Ng* denotes *N. gonorrhoeae*, *Ec*: *E. coli* and *Pa*: *P. aeruginosa*.

Most mutational data exist for *H. influenza* and *N. gonorrhoeae* and to a lesser extent in *P. aeruginosa*; the relevant clinical mutations typically cluster within one of the five regions described above (Fig. 5a and b). Fewer mutations have been observed in *E. coli* PBP3, and only a few examples of target-mediated resistance among *E. coli* clinical isolates are reported in the literature.

Target-mediated resistance in *P. aeruginosa* PBP3, *H. influenzae* PBP3 and *N. gonorrhoeae* PBP2

A review by Clark *et al.* [28] found that 60% of the studied clinical isolates of *P. aeruginosa* contained the PBP3 mutation ^{Pa}R504C/H and that this mutation (alongside others) decreased susceptibility to four of the six β-lactams tested. ^{Pa}R504C/H is present in at least one isolate reported in 7 of the 11 papers covered in this review. ^{Pa}R504 sits right at the start of the β4 sheet (Fig. 2a) and confers reduced acylation rate toward bocillin *in vitro* (Fig. 2b). Two other common resistance-mediating mutations in *Pa*PBP3 are ^{Pa}P527S/T and ^{Pa}G531D/E [28], which are located on the β5–α11 loop (Fig. 5c). No mutations have been reported in the β2b–β2c–β2d, α10–β3 and α5–α6 regions of *Pa*PBP3 from clinical isolates (Table 2).

The *Hi*PBP3 mutations for which data are readily available and which have consistently been shown to affect resistance in the literature are ^{Hi}S357N in the β2b–β2c–β2d region (more specifically in the β2b–β2c loop); ^{Hi}R501L, ^{Hi}A502V and ^{Hi}V511A in the α10–β3 region; ^{Hi}R517H and ^{Hi}N526K in the β3–β4 region; ^{Hi}S385T, ^{Hi}L389F and ^{Hi}M377I in the α5–α6 region; and ^{Hi}G555E and ^{Hi}Y557H in the β5–α11 region (Fig. 5d). References and proposed effects of these mutations are summarized in Table 3.

In the case of *Ng*PBP2, as many as 85 amino residues have been observed to be altered [55]. Four clinically relevant alterations, ^{Ng}F504L, ^{Ng}A510V, ^{Ng}A516G [56] and ^{Ng}N512Y [49], have been identified in the β3–β4 region (Fig. 5e). In a study investigating 98 clinical isolates, Whiley *et al.* [25] determined that either ^{Ng}G542S or ^{Ng}P551S/L in the β5–α11 region was consistently associated with decreased ceftriaxone susceptibility and penicillin resistance (Fig. 5e). Moreover, the aspartate insertion ^{Ng}D346a in the β2b–β2c–β2d region (more specifically in the β2c–β2d loop), already discussed in the above section about the *Ng*TP2$^{HR-6140}$ structure, is known to confer penicillin resistance.

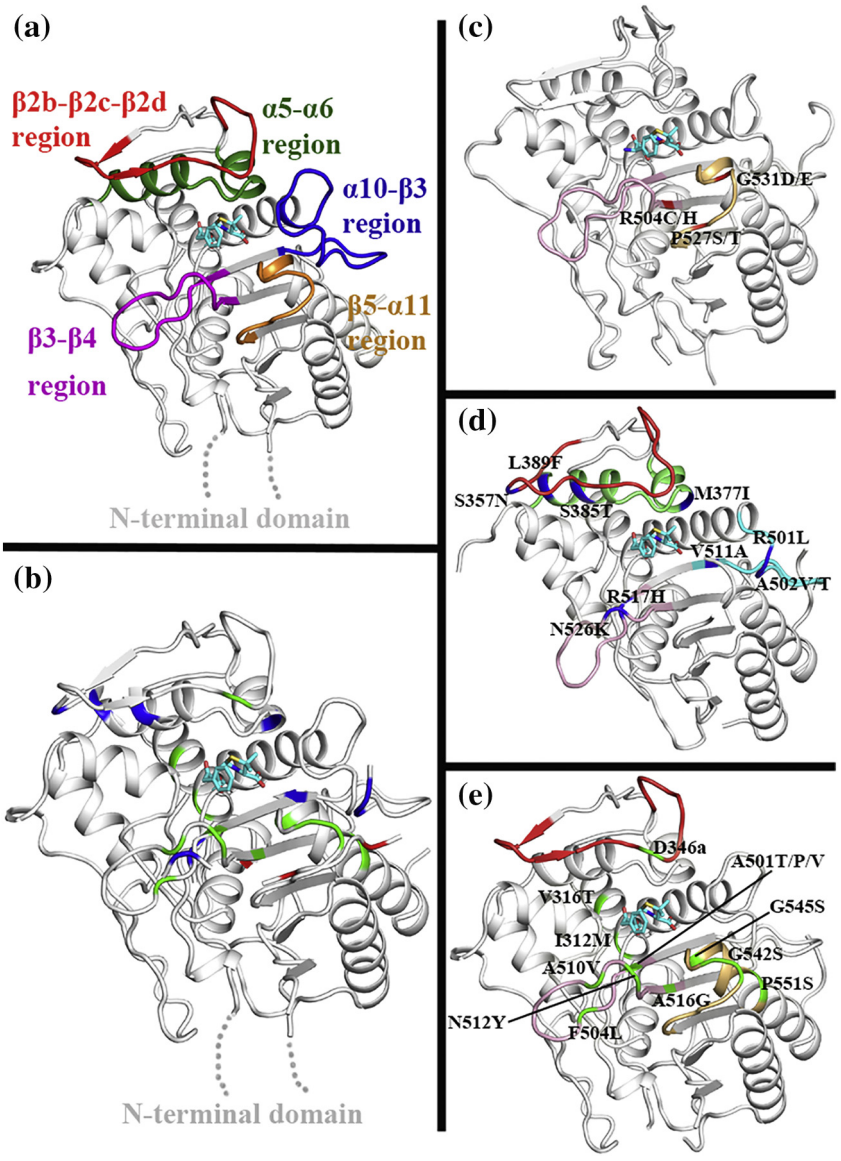

Fig. 5. Mapping of frequently occurring resistance mutations on PBP3s. (a) The most common regions containing resistance mutations in PBP3s are highlighted in different colors and labeled; the model structure used here is that of *Ng*TP2$^{HR-6140}$. (b) *Ng*TP2$^{HR-6140}$ structure-aided visualization of the most common resistance mutations in various PBP3s placed on a single structure; the model structure used here is that of *Ng*TP2$^{HR-6140}$. Resistance mutations occurring in *Pa*PBP3, *Hi*PBP3 and *Ng*PBP2 are colored red, blue and green, respectively. Panels c, d and e show labeled resistance mutations in the transpeptidase domain structures of *Pa*PBP3, *Hi*PBP3 and *Ng*PBP2, respectively. All structures are colored white with mutations colored red, blue and green for *Pa*PBP3, *Hi*PBP3 and *Ng*PBP2, respectively. The regions containing the mutations are also highlighted with colors corresponding to panel a but in lighter shades. Penicillin G, represented in cyan stick, is superimposed in the catalytic pocket of structures in all five panels for reference.

No mutations have been reported in the α10–β3 and α5–α6 regions of *Ng*PBP2 from clinical isolates.

Resistance-aiding mutations in *E. coli*

Alm *et al*. [29] have recently reported insertions of either ^{Ec}YRIN or ^{Ec}YRIK after ^{Ec}P333 in *Ec*PBP3 of *E. coli* New Delhi MBL (NDM-1) clinical isolates conferring 32-fold increases in the MIC values of aztreonam, cefpodoxime and cefepime, and moderate increases to the other cephalosporins tested, amoxicillin and ampicillin when it was reconstructed into an isogenic strain. The ^{Ec}YRI(N/K) insertion appears to be a duplication of residues ^{Ec}Y334–R335–I336–N337 [29] in the β2b–β2c–β2d region (more specifically in the β2b–β2c loop), the same location as the ^{Hi}S357N mutation in *Hi*PBP3 (see above) (Fig. 6). A further clinical isolate of *E. coli* has been reported with the PBP3 gene containing an insertion as a result of a perfect gene duplication of four residues, TIPY, after ^{Ec}Y334 [77]. It is interesting to note that the ^{Ec}TIPY and ^{Ec}YRI(N/K) insertions are overlapping one another in sequence alignment. A literature search found no other examples of clinical isolates of *E. coli* with mutations to PBP3. The low incidence of PBP3 mutations in *E. coli* isolates may be due to observations that in *E. coli* β-lactamases are the primary mechanism of resistance to β-lactams [57].

It is important to note that superposition of different subunits from the asymmetric units of crystals of NgTP2 (two subunits) (Fig. SI 11) and HiTP3 (four subunits) (Fig. SI 12) shows conserved conformations among the overall structure (rmsd of 0.15 and 0.5 Å on average, respectively) and in particular the

Table 2. Summary of the regions and mutations in *P. aeruginosa*, *H. influenzae*, *N. gonorrhoeae* PBP3/2 we highlight in this study

Region	*P. aeruginosa PBP3*	*H. influenzae PBP3*	*N. gonorrhoeae PBP2*
β2b–β2c–β2d	–	^{Hi}S357N	^{Ng}D346a insertion
α10–β3	–	^{Hi}R501L, ^{Hi}A502V, ^{Hi}V511A	–
β3–β4	^{Pa}R504C/H	^{Hi}R517H, ^{Hi}N526K	^{Ng}F504L, ^{Ng}A510V, ^{Ng}A516G, ^{Ng}N512Y
α5–α6	–	^{Hi}S385T, ^{Hi}L389F, ^{Hi}M377I	–
β5–α11	^{Pa}P527S/T, ^{Pa}G531D/E	^{Hi}G555E, ^{Hi}Y557H	^{Ng}G542S, ^{Ng}G545S, ^{Ng}P551S/L

resistance-mediating mutation-carrying loops discussed in this work, validating the differences discussed in the structural comparisons below.

Discussion

Alongside the publication of the first crystal structures of PBP3 TP domains from *H. influenzae,* we aimed to map and rationalize the effects of PBP3 mutations not only in *H. influenzae* but also in other gram-negative PBP3s and their impact upon resistance to β-lactam antibiotics. The following discussion will aim to (1) compare frequently reoccurring mutations across different species within the five "hotspot" regions identified in the Results section and (2) try to rationalize how resistance may be achieved through such mutations.

Mutations in the β2b–β2c–β2d region of PBP3s

The ^{Ng}D346a insertion in the β2c–β2d loop was shown to have 5-fold decrease in the binding of [^{14}C] penicillin G [31]. In an analysis by Whiley *et al*. [58], only 4 out of 95 strains containing the ^{Ng}D346a insertion were penicillin G susceptible. Therefore, although ^{Ng}D346a alone is not sufficient to confer high enough levels of protection against penicillin, it does appear to be a key step in the development of resistance in *Ng*PBP2 [22]. Moreover, the introduction of other amino acids at this position, in some cases lowering penicillin acylation rates in *in vitro* assays with the purified recombinant proteins [59], did not lead to viable resistant strains [59,60]. These experiments indicated that the properties of the extra aspartate specifically allow a balance between decreased β-lactam acylation and acceptable transpeptidation rates, rather than just acting as a spacing residue to induce an effect mediated further down the loop. Fedarovich *et al*. [30] have shown using a docked model that the side chain of the inserted

Table 3. Summary of selected mutations in *H. influenzae* PBP3.

Region	Mutation	Class it defines [26,27]	Chronology [47]	Resistance conferred	Suggested mechanisms of resistances	Citations (further citations in text)
β3–β4	^{Hi}R517H	I	1st	Cephalosporins and penicillins (low)	Direct interaction with R1 side chain; effect related to change in p*K*a; long-range structural re-arrangements	[46,48]
β3–β4	^{Hi}N526K	II	1st	Cephalosporins and penicillins (low). Carbapenems (high)	Long-range structural re-arrangements	[46,48]
α5–α6	^{Hi}S385T	III/III-like	2nd	Cephalosporins (high). Penicillin (low)	Indirect steric hinderance of the active site	[46,47]
α5–α6	^{Hi}L389F	III/III-like	3rd	Cephalosporins (high)	Indirect steric hinderance of the active site	[46,47]
α5–α6	^{Hi}M377I	III/III-like	–	Unclear	Epistatic effect	[46,49]
β2b–β2c–β2d	^{Hi}S357N	–	–	Cefuroxime (high)	Indirect steric hinderance of the active site	[50]
α10–β3	^{Hi}A502V/T	IIb/c	–	Penicillins (intermediate).	Influence on K(T/S)GT motif	[50–52]
α10–β3	^{Hi}V511A	–	–	Amoxicillin (high). Cephalosporins (intermediate)	Influence on K(T/S)GT motif	[50,53]
α10–β3	^{Hi}R501L	–	–	Cefuroxime	Influence on K(T/S)GT motif	[50]
β5–α11	^{Hi}G555E	–	–	Cefotaxime	Changes to the hydrophobic wall	[54]
β5–α11	^{Hi}Y557H	–	–	Cefotaxime	Chanes to the hydrophobic wall	[54]

aspartate sits near the hydroxyethyl of acylated meropenem. The authors rationalized the observed 16- and 5-fold decrease in MICs of strain 6140 for penicillin G and meropenem, respectively, by suggesting that the more hydrophobic region of penicillin G in this area will be affected by the presence of the negative charge on ^{Ng}D346a to a greater extent than the more polar hydroxyethyl group of meropenem (Fig. SI_1). While the apo structure of *Ng*TP2$^{HR-6140}$ with improved resolution reported in this study highlighted the flexible nature of the β2c–β2d loop, it did not offer new insights into the mechanistic implication of resistance through insertion of ^{Ng}D346a. However, it could be exploited in the future to obtain highly detailed structures of β-lactam-*Ng*TP2$^{HR-6140}$ adducts to monitor the interactions between ^{Ng}D346a and inhibitors.

After identifying a series of *E. coli* clinical isolates with higher-than-expected aztreonam/avibactam resistance, Alm *et al*. [29] discovered insertions of either YRIN or YRIK after ^{Ec}P333 in PBP3. The Y334–R335–I336–K337 insertion raised the resistance to aztreonam/avibactam slightly above that of YRIN. Since the YRI(N/K) insertion occurs in the β2b–β2c loop, part of the β2b–β2c–β2d region that forms the roof of the catalytic pocket (Fig. 6), the authors attributed the effect of this mutation to a restriction of the active-site cleft. As a result, all β-lactams with a large R1 group (Fig. SI_1) would be expected to be affected by this insertion, which is in agreement with the findings that carbapenem MICs were unaffected [29]. Unfortunately, the wild-type *Ec*TP3 structure with improved resolution reported here cannot provide new insights into the effect of the YRI(N/K) insertion. This hypothesized resistance mechanism is similar to the one proposed by Straker *et al*. [50] to explain the effect of the ^{Hi}S357N mutation on MIC values in *H. influenzae*. The authors used a homology model build by threading onto Streptococcus pneumonia PBP2X (PDB code 1QMF) to conclude that the increased bulk of the asparagine, compared to serine, would induce hinderance by leading the β2b–β2c–β2d loops to push into the active-site cleft and restricting access to the β-lactams (Fig. 6). The authors justified this prediction by asserting that the mutation is only found in strains with a high-level resistance to the bulky cephalosporin cefuroxime [26]. While the similar resistance mechanisms suggested for the ^{Ec}YRI(N/K) insertion and ^{Hi}S357N mutation are plausible, such a steric effect is likely to have highly damaging consequences to functional transpeptidation, which were not tested. The novel crystal structure of *Hi*TP3 presented in this study opens up the possibility of crystallization of the ^{Hi}S357N mutant of *Hi*PBP3 in order to investigate the conformational changes driven by this mutation.

Mutations in the α10–β3 region of PBP3s

Mutations in the α10–β3 region of PBP3 have only been observed in clinical isolates of *H. influenzae* and include ^{Hi}A502T/V, ^{Hi}V511A and ^{Hi}R501L (Fig. 5c). The α10–β3 region is near to the conserved KTG sequence, which contains the catalytic lysine **K_2** (K512 in *H. influenzae* PBP3). The residues in this region form the binding pocket for the highly conserved carboxylic acid group of β-lactams [5,61]. The frequent appearance of mutation ^{Hi}A502T/V alongside ^{Hi}N526K prompted

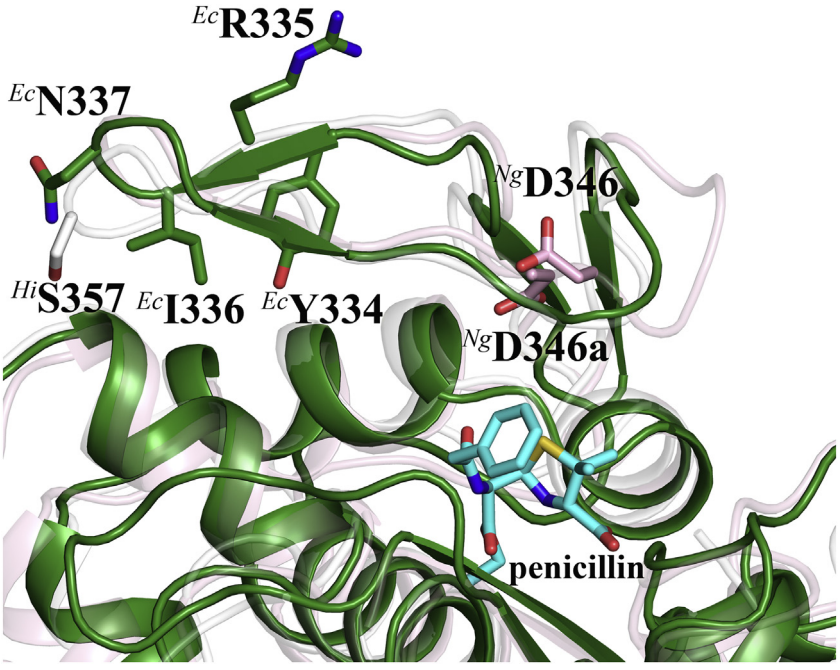

Fig. 6. Comparison of the β2b–β2c–β2d region between TP domain structures of *Ec*PBP3 (green), *Hi*PBP3 (white) and *Ng*PBP2 from penicillin resistant strain FA6140 (pink). Residues discussed in the main text are shown in sticks and labeled. Penicillin G, represented in cyan stick, is superimposed in the catalytic pocket of all three structures for reference.

Dabernat *et al*. [27] to further expand on the classification of Ubukata *et al*. [26], introducing four subgroups: subgroup IIb is defined by the presence of ^{Hi}N526K + ^{Hi}A502V, whereas subgroup IIc is defined by ^{Hi}N526K + ^{Hi}A502T. García-Cobos *et al*. [51] observed that while IIb and IIc mutations had around 4-fold increases in the MIC of ampicillin and amoxicillin-clavulanic acid compared to the wild type, these had little effect on the MICs of oral cephalosporins, which were only affected by mutations characteristic of group III and group III-like (Table 3). Similar observations were made by Straker *et al*. [50], who noted that the ^{Hi}N526K + ^{Hi}A502T was insufficient to give resistance to cefuroxime. Fluit *et al*. [52] have also reported a high frequency of ^{Hi}N526K + ^{Hi}A502V/T strains, which exhibit amoxicillin and ampicillin resistance.

Straker *et al*. [50] showed that transformants of ^{Hi}V511A + ^{Hi}R517H were resistant to cefuroxime and the level of resistance was greater than that observed for the clinical strain. Comparing cephalosporin- and ampicillin-resistant isolates with and without ^{Hi}V511A to each other, the authors showed that the introduction of the ^{Hi}V511A mutation leads to a further doubling in the MICs of ceftizoxime and cefpodoxime, but there was no change to ampicillin resistance. In contrast, Barbosa *et al*. [62] determined that ^{Hi}V511A mutations correlated with resistance to ampicillin, cefepime and amoxicillin/clavulanic acid, although they lacked the data to determine this conclusively. Kishii *et al*. [53] produced transformants of clinical strains with or without ^{Hi}V511A mutations, alongside other mutations, showing that in both clinical and transformed strains, the addition of ^{Hi}V511A had no effect on resistance to ampicillin or cefditoren but had a 4-fold increase in the resistance to cefdinir and a 16-fold increase in the resistance to amoxicillin. This difference in response to ampicillin and amoxicillin is intriguing since these drugs differ by a single oxygen (Fig. SI_1), which is significantly distant from the ^{Hi}V511 residue (Fig. SI_8). Barbosa *et al*. [62] observed ^{Hi}V511A and ^{Hi}A502T occurring simultaneously in two strains, although they did not report the effect of the double mutation on MIC values. Mutation ^{Hi}R501L was reported for the first time by Straker *et al*. [50] as conferring a high level of resistance to cefuroxime when it alone was mutated. Surprisingly, the double mutant ^{Hi}N526K + ^{Hi}R501L showed an MIC against cefuroxime at least 4-fold lower than ^{Hi}R501L alone. It is interesting to note that ^{Hi}R501S, a small polar substitution (serine) rather than a bulkier hydrophobic one (leucine), was categorized as a non-resistance defining mutation by Aguirre-Quinonero *et al*. [63], whereas its neighboring residue (^{Hi}A502) can develop resistance by changing to either valine or threonine. Overall, the evidence reported on resistance-aiding mutations in the α10–β3 region of *Hi*PBP3 is quite complicated and at times even controversial. Unfortunately, the *Hi*TP3^{FEKQ} alone presented here cannot explain the effects on the MICs observed for these mutations and some of their combinations. However, structures of β-lactam-*Hi*TP3^{FEKQ} adducts may in the future help to understand the molecular correlations between these mutations and the MICs.

Although resistance-aiding mutations in the α10–β3 region of PBP3 have only been observed in clinical isolates of *H. influenzae*, α10–β3 region mutants in other organisms have been produced by *in vitro* passage with β-lactams. For example, one of the mutations produced with ertapenem passage in *E. coli*, ^{Ec}A484V [57], aligns to ^{Hi}A502V/T, a *H. Influenza* mutation capable of producing meropenem resistance [62]. While the mutations in each case are insufficient to produce carbapenem resistance when expressed in PBP3 alone, the coincidence of the alanine to valine mutation indicates a similar underlying mechanism. The presentation of high-resolution structures in this work for both *Hi*TP3 and *Ec*TP3, as well as other TP domain of PBP3 from different pathogenic organisms, could result in being an invaluable tool for cross validation of superposing mutations, such as ^{Hi}A502V/T and ^{Ec}A484V, among the different species.

Mutations in the β3–β4 region of PBP3s

The β3–β4 loop has been suspected for a number of years to be functionally important as it is the site of various clinically relevant mutations in pathogenic species. Skaare *et al*. [47] suggested that the first stage of β-lactam PBP3-mediated resistance development in *H. influenzae* is the acquisition of either ^{Hi}R517H or ^{Hi}N526K, located at the end of the β3 strand and the beginning of β4 strand, respectively (Fig. 5d). These two key mutations are frequently observed, as many as 93.2% of 236 clinical *Hi*PBP3 mutants comtained of the two mutations [51]. Mutations ^{Hi}R517H and ^{Hi}N526K are often reported to be mutually exclusive, although a strain containing both mutations has been isolated [48]. Simultaneous transformation of both mutations into a recombinant strain did not produce any deleterious effect and even slightly increased the MIC against imipenem [46]. However, in a ^{Hi}R517H-^{Hi}N526K double mutant clinical isolate, imipenem resistance was not shown to have increased compared to ^{Hi}R517H-only strains [48]. Therefore, although ^{Hi}R517H and ^{Hi}N526K appear to be "central to phenotypical resistance" [64], data in both recombinant studies [46,65] and clinical isolates [48] indicate that these residues only lead to the low resistance in the absence of other mutations. Structurally (this work), ^{Hi}R517H and ^{Hi}N526K lie close to each other, extending into the active-site cleft in a region around 15 Å from the active-site serine, $\mathbf{S_1}$ (^{Hi}S327). Superposition of ceftazidime-PaPBP3* adduct (PDB code 3PBO) indicates that the R1 chains of β-lactam inhibitors tend to extend into this region so direct interactions

may be possible with ligands in some cases (Fig. 7a). Sanbongi *et al*. [48] attributed the high ceftazidime resistance of ^{Hi}R517H mutations (but not ^{Hi}N526K mutations) to direct interactions of the R1 chain with the histidine residue. Osaki *et al*. [46] observed an 8-fold increase in the MIC against imipenem with the ^{Hi}N526K mutation alone (but strangely no change in meropenem MIC), and Sanbongi *et al*. [48] reported high imipenem and meropenem resistance in ^{Hi}N526K, but not ^{Hi}R517H mutations. However, due to the lack of extended R1 chains in carbapenems (Fig. 7b), mechanisms involving direct interaction cannot be justified and remain an unsolved problem, even with the novel structure of the *Hi*TP3 presented here. Interestingly, the signature ^{Sp}Q552E mutation in *Streptococcus pneumoniae* PBP2X [24] (PDB code 1RP5) aligns with ^{Hi}R517 (Fig. SI_9), and this mutation was shown to have a decreased acylation rate of both penicillin and cefotaxime in purified recombinant proteins [24,66]. ^{Sp}Q552E was structurally investigated by Pernot *et al*. [66] assigning the increased resistance in these strains to the introduction of a negative charge by the glutamic acid. At pH 7, arginine is positively charged, while histidine is neutral, so an alternative explanation may be that steric hindrance due to a shorter, bulkier and less flexible rotamer such as histidine, rather than difference in charge, is the cause for decrease binding affinity in the R517H *Hi*PBP3 mutant.

Due to a differential increase in MICs of cefotaxime, cefditoren and cefcapene (Fig. SI_1) following the acquisition of a ^{Hi}N526K mutation, Osaki *et al*. [46] proposed that the lower resultant MIC against cefditoren in a ^{Hi}N526K strain compared to cefotaxime and cefcapene must be due to a feature of its R2 chain, since the three drugs have the same R1 chains but different R2 chains. However, as shown in Fig. 7a, ^{Hi}N526 occurs near the end of long R1 chains, highly distant from the binding pocket of R2 chains. Besides direct interactions between mutations and inhibitors, it is also possible that ^{Hi}R517H and ^{Hi}N526K lead to resistance through mechanisms involving conformational changes of the β3–β4 loop. In *S. pneumoniae,* failure to observe electron density in the β3–β4 loop of PBP2b led Contreras-Martel *et al*. [67] to conclude that mutations in this region can enhance structural flexibility in the loop, which could increase resistance. The flexible nature of the β3–β4 loop has been reported in other cases as well. In *Pa*PBP3* structures, electron density for this loop in the crystals of the apo form has never been observed, but can be seen in some cases when β-lactams with bulky R1 chains are bound [33,68] (and this work, Fig. 1a). However, electron density of the β3–β4 loop is clearly visible in all four copies of apo *Hi*TP3^{FEKQ} in the asymmetric unit. Therefore, the structure of *Hi*TP3^{FEKQ} might allow in future to study the effects of ^{Hi}R517H and ^{Hi}N526K mutations on the flexibility of the β3–β4 loop, in the presence and absence of bound β-lactams; with the caveat though that, in all four copies of *Hi*TP3^{FEKQ}, the β3–β4 loop is engaged in identical crystallographic contacts (Fig. 1d). Other, far less common, mutations observed in this region of *Hi*PBP3 include ^{Hi}Y528H [50,69] and ^{Hi}N526H [70]. Thegerström *et al*. [69] produced a transformed ^{Hi}Y528H strain and observed small decreases in the ampicillin susceptibility, on a similar scale to those observed in transformed ^{Hi}N526K strains [46].

The ^{Hi}R517H or ^{Hi}N526K substitutions, thought to be an important initial step in the development of resistance to both penicillin and cephalosporins, structurally align, respectively, to ^{Ng}A501 and ^{Ng}A510 sites of mutation in *Ng*PBP2 (Fig. SI_10). ^{Ng}A501 has been found in clinical isolates mutated to valine, threonine and proline, and is associated with cephalosporin resistance in mosaic and non-mosaic strains [32]. Particularly, ^{Ng}A501P elevated the MIC of cefixime and ceftriaxone but decreased resistance to penicillin G in wild-type strains, which had been transformed with the mosaic *penA35* allele of PBP2. How this mutation can provide such drug specificity has not been determined. Powell *et al*. [31] determined that three β3–β4 loop (^{Ng}F504L, ^{Ng}A510V and ^{Ng}A516G) and one β5-β11 loop (^{Ng}P551S) mutations decreased the acylation rates of [^{14}C]penicillin G 5-fold in a recombinant protein compared to the wild type. However, similar results were obtained having just two of those four substitutions, ^{Ng}F504L and ^{Ng}P551S, suggesting that these were the important determinants of resistance [31]. Another *Ng*PBP2-mediated resistance mutation reported in the β3–β4 loop is ^{Ng}N512Y [32]. In order to rationalize the effects of multiple simultaneous mutations observed in mosaic *N. gonorrhoeae* PBP2, Nabu *et al*. [55] used proteochemometric modeling, correlating data on mutations to the effect on MIC and using this model to make accurate predictions. Their data showed that mutations in the β3–β4 loop (^{Ng}F504L, ^{Ng}A501V and ^{Ng}A516G), as well as the β5–α11 loop (^{Ng}P551L/S and ^{Ng}G542A), correlate with increased MICs to penicillin, cefixime and ceftriaxone. In agreement with more recent data by Tomberg *et al*. [32], Nabu *et al*. [55] strikingly predicted that *Ng*A501P would decrease resistance to penicillin G.

A disordered β3–β4 loop could not be fitted in the wild-type structure of *Ng*PBP2*; however, electron density is very clear in both molecules of *Ng*TP2$^{HR\text{-}6140}$ in the asymmetric unit. Importantly, unlike in the case of the *Hi*TP3^{FEKQ} and *Ng*TP2$^{t3–6140}$ (PDB code 4U3T) [30] structures, the β3–β4 loop in the structure of *Ng*TP2$^{HR\text{-}6140}$ is not engaged in crystallographic contacts (Fig. 1c). It should also be noted that the β3–β4 loop could only be fitted in one (molecule A) of the two molecules in the lower-resolution structure of *Ng*TP2$^{t3–6140}$.

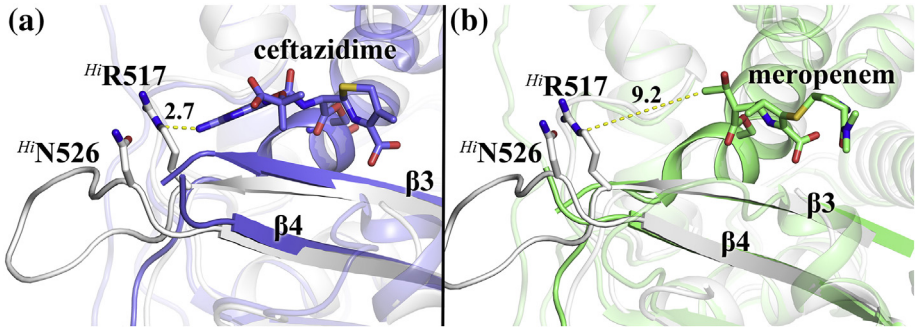

Fig. 7. Potential interactions between residues ^{Hi}R517 and ^{Hi}N526 of *Hi*PBP3 with cephalosporins and carbapenems. Superposition of TP domains from structures of apo *Hi*TP3^{FEKQ} (white) with (a) ceftazidime-acylated *Pa*PBP3* (purple) and (b) meropenem-acylated *Pa*PBP3* (green). ^{Hi}R517, ^{Hi}N526 and inhibitors are represented in sticks and labeled. Distances are shown with yellow dashed lines and labeled in Å.

The substitution ^{Pa}R504C/H has been frequently reoccurring in *P. aeruginosa* isolates from cystic fibrosis patients, and alongside other mutations, it was found to decreased susceptibility to four of the six tested β-lactams [28]. The ^{Pa}R504C/H mutation sits right at the start of the β4 sheet, structurally aligning with ^{Ng}A516 (Fig. 8); therefore, it may influence β-lactam affinity with similar mechanisms as some of the *H. influenzae* and *N. gonorrhoeae* mutations discussed above. Since the side chain of ^{Pa}R504 is pointed downward with respect to the catalytic pocket, it is unlikely that this mutation may act *via* direct interactions with the inhibitors, but it seems more plausible an effect on the β3–β4 loop conformation. However, superposition of the structures of wild type *Pa*PBP3* and mutant *Pa*PBP3*^{R504C} did not show any difference when comparing either the apo or piperacillin-acylated pair, with RMSD of 0.4 and 0.3 Å, respectively (see the Results section). It should be noted that in comparing the wild-type forms, the β3–β4 loop is completely not visible (as discussed above in case of *Pa*PBP3* apo structures), from residue 490 (immediately after strand β3) to residue 503 (just before strand β4), whereas in piperacillin-acylated structures, it is well defined, identical in conformation (Fig. 2a) and not engaged in any crystallographic contacts (Fig. 1a).

The decreased acylation rate observed in our bocillin data (Fig. 2b) indicates that the ^{Pa}R504C mutation is having an effect on β-lactam binding. However, as with previous reports comparing structural and kinetic data [31,32], obvious, large-scale structural changes resonsible for these effects are not apparent in the static crystallographic models.

Mutations in the α5–α6 region of PBP3s

Mutations in the α5–α6 region (Fig. 5a and b) have only been reported for *Hi*PBP3 and include ^{Hi}S385T, ^{Hi}L389F and ^{Hi}M377I. According to Skaare *et al*. [47], these are second-stage substitutions, occurring in strains already expressing either ^{Hi}R517H or ^{Hi}N526K mutations in the β3–β4 loop (see above) and increasing further cephalosporin resistance compared to isolates possessing only ^{Hi}R517H or ^{Hi}N526K mutations. The combination of either ^{Hi}R517H or ^{Hi}N526K with ^{Hi}S385T, ^{Hi}L389F and ^{Hi}M377I mutations in *H. influenzae* clinical isolates correlates with very high resistance to certain cephems such as cefotaxime and cefpodoxime, but with ampicillin and carbapenem resistance comparable to strains carrying only ^{Hi}R517H or ^{Hi}N526K mutation [51]. Some researchers consider the ^{Hi}L389F mutation as a third stage of resistance as they noted further resistance to the cephalosporins in strains containing the additional ^{Hi}L389F mutation [47], whereas other sources have controversially reported no decrease in cephalosporin susceptibility in strains lacking only the ^{Hi}L389F mutation [62]. To investigate the role played by the ^{Hi}S385T, ^{Hi}L389F and ^{Hi}M377I mutations, Osaki *et al*. [46] created 12 recombinant strains combining these plus ^{Hi}R517H or ^{Hi}N526K mutations. MICs of these strains showed that subsequent insertion of ^{Hi}N526K and then ^{Hi}S385T mutations each resulted in a doubling of the ampicillin MICs, but further addition of ^{Hi}L389F and/or ^{Hi}M377I had no effect. For the cephalosporins, subsequent addition of ^{Hi}N526K, followed by ^{Hi}S385T and ^{Hi}L389F each led to increases in cephalosporin resistance, with the extent depending on the type of cephalosporin tested. Similar observations were made for the addition of ^{Hi}L389F into a ^{Hi}R517H + ^{Hi}S385T recombinant strain. Addition of ^{Hi}M377I to any strain tested did not increase MICs for most cephalosporins, ampicillin or carbapenems and consistently led to increased cefaclor susceptiblity [46]. Therefore, ^{Hi}M377I mutation, which is frequently observed alongside ^{Hi}S385T and ^{Hi}L389F and designated by some reports as being important for conferring high-

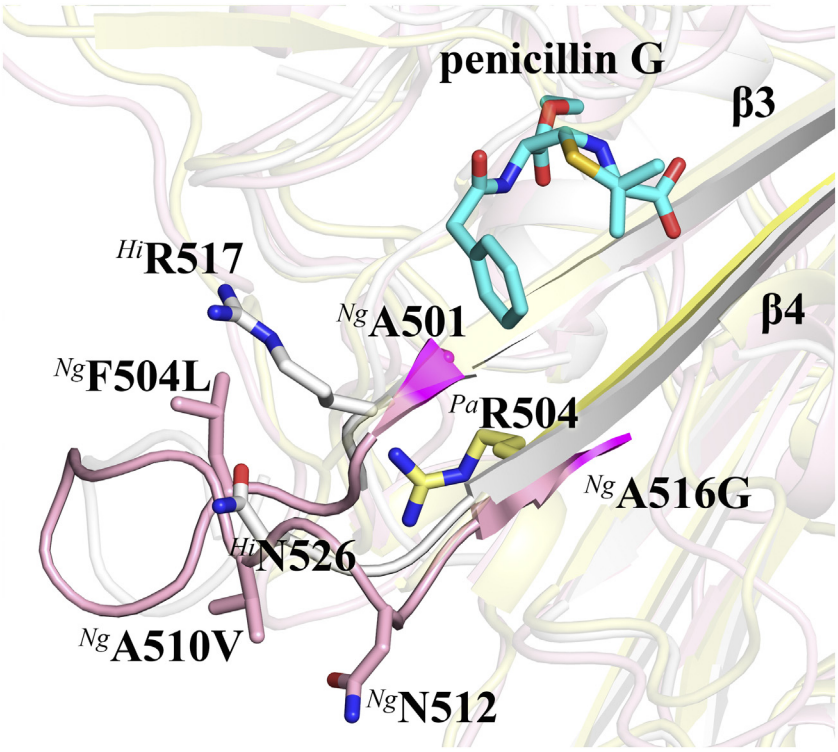

Fig. 8. Comparison of resistant mutations in the β3–β4 region of TP domains from *Pa*PBP3 (yellow), *Hi*PBP3 (white) and *Ng*PBP2 (pink). Mutating residues are represented in sticks and labeled. Penicillin G, represented in cyan stick, is superimposed in the catalytic pocket of all three structures for reference.

level cephalosporin resistance [64], may instead have epistatic effects.

The structure of *Hi*TP3^{FEKQ} presented here shows that ^{Hi}M377I is located at the end of helix α5, while ^{Hi}S385T and ^{Hi}L389F are located around the middle of helix α6, where helices α5 and α6 sit on top of the inhibitor (Fig. 5d). The short 3-residue α5–α6 loop is the site of the catalytic motifs, SXN, containing **S_2** and **N**. Therefore, mutations in those positions have the potential to displace either the roof of the active-site and/or catalytic residues in the SXN motif, which in turn are likely to affect inhibitor affinity. While the wild-type structures presented here cannot answer these questions, our results offer the possibility if crystallizing recombinant *Hi*PBP3 containing the three substitutions in the α5–α6 region plus either the ^{Hi}R517H or ^{Hi}N526K mutation to assess conformational changes that may explain the resistance mechanism.

Mutations in the β5–α11 region of PBP3s

Han *et al*. [71] have discussed how the β5–α11 loop in *Pa*PBP3 is the site of a large conformational change in the presence of aztreonam and ceftazidime. Residues ^{Pa}Y532 and ^{Pa}F533 within this loop are displaced significantly from their apo positions to form an aromatic wall alongside ^{Pa}Y503, and this hydrophobic patch helps stabilize the gem-dimethyl group found in both antibiotics. These results are in agreement with the observations from the higher resolution apo and amoxicillin-bound PaPBP3* structures presented in this study. Two commonly mutations reoccurring in PaPBP3 from clinical isolates of cystic fibrosis patients are ^{Pa}P527S/T and ^{Pa}G531D/E, which are located on the β5–α11 loop. These mutations are likely to influence the flexibility of this region and hence the degree of stability provided by this region to β-lactams with hydrophobic groups at this point.

There are two glycine to serine mutations, ^{Ng}G542S and ^{Ng}G545S [55], in the β5–α11 loop of *Ng*PBP2 from clinical isolates, which sit either side of two tyrosine residues, ^{Ng}Y543 and ^{Ng}Y544, that align with ^{Pa}Y532 and ^{Pa}F533. These two mutations will likely reduce the number of possible conformations of the β5–α11 loop, as flexible glycines are replaced by more sterically hindered serines. However, in the case of *Ng*PBP2, it is unclear whether this conformational change of the β5–α11 loop is relevant since there are no ^{Ng}PBP2 structures with a β-lactam bound and this region. Takahata *et al*. [72] also describe ^{Ng}G545S as a primary mutation leading to a small increase in cephem resistance in mosaic PBP2, which could then enhance resistance further with the acquisition of ^{Ng}I312M and ^{Ng}V316T (note that these two mutations are found on helix α4, which does not belong to any of the regions highlighted here; no other mutations have been reported on helix α4 among other species). According to the structures of different *Ng*PBP2 constructs presented and

reviewed in this work, the ^{Ng}G545S mutation will introduce an extra hydroxyl group into the β-lactam acid group binding pocket, which may affect affinity directly. However, studies by Tomberg *et al*. [49] investigating these three mutations found little effects on resistance when introduced into a wild-type strain, leading the authors to suggest that they may have a stabilizing role on the structure rather than direct interactions with inhibitors. The higher resolution of *Ng*TP2$^{HR-6140}$ presented here may assist, due to probably more stable crystal contacts than in the case of previous lower-resolution structures, in obtaining structures of these mutants.

Recent work has identified two mutations within the β5–α11 region of *H. Influenza* PBP3, capable of producing decreased susceptiblity to cefotaxime, without concomitant increases in ceftriaxone resistance [54]. In transformant strains expressing background group III mutations to *Hi*PBP3 (Table 3), the authors observed that the introduction of both ^{Hi}G555E and ^{Hi}Y557H raised the MIC to cefotaxime 32-fold. Introduction of either of these mutations individually had more limited effects. As with ^{Pa}G531D/E and ^{Ng}G542S, which align closely, ^{Hi}G555E is likely to influence the flexibility of the β5–α11 region and the formation of the aromatic wall. Since ^{Hi}Y557 genetically aligns to ^{Pa}Y532, the tyrosine to histidine substitution is also likely to influence the aromatic wall. This region could not be built in the apo *Hi*TP3^{FEKQ} structure due to high flexibility. Therefore, β-lactam-acylated structures may be required to rigidify this region and allow structural investigation of these mutants.

Conclusions

This work examines the role of PBP3 (and PBP2) mediated resistance in four gram-negative species: *H. influenzae, N. gonorrhoeae, E. coli* and *P. aeruginosa,* for which we have solved either novel or improved resolution crystal structures. *Hi*PBP3 and *Ng*PBP2 were found from the literature to have, by far, the most data on clinical mutations, whereas only very few examples of PBP3 clinical mutations could be identified in *E. coli* and *P. aeruginosa*. However, five hotspots were identified on the TP domain of PBP3/PB2 where these mutations are frequently reoccurring among different species: (1) the β2b–β2c–β2d region, (2) the α10–β3 region, (3) the β3–β4 region, (4) the α5–α6 region and (5) the β5–α11 region. The coincidence of mutations in these regions presents the possibility for overlapping molecular resistance mechanisms of mutations from different species. Moreover, this work highlights the correlation in some cases between the region where the mutations occurred and the type of β-lactams for which resistance developed. For example, ^{Ng}D346a insertion in the β2c–β2d loop provides penicillin G but not cephalosporin resistance, whereas second stage mutations in the α5–α6 region of *Hi*PBP3 only contribute to increase cephalosporins resistance but not ampicillin. However, despite PBP3 (and PBP2 from *N. gonorrhoeae*) proteins having a large degree of structural and functional similarity and being targeted by a similar set of drugs, the variety of the reported resistance mutations among the species is quite significant. These inter-species variations may reflect the differences in natural muropeptide substrates processed by the protein, highlighting the need to develop quantitative PBP3 assays with natural substrates to progress our understanding of the biological price of resistance and how this may be effectively compensated. Other mechanisms occurring simultaneously, small differences between the structures, differences in the frequency of mutations between species, differences in drugs specificity, and/or differences in the prescribing practices in each disease are also variables that need to be taken into account. Therefore, understanding the effect mutations have on resistance by observing crystal structures is not easy as these can only provide a static model, failing to show the dynamics which mutations may introduce or remove not only in the presence of β-lactams but also in the presence of natural substrates, about which we still know very little. The abundance of substitutions outside of the active site indicates that mutations are rarely leading to resistance *via* direct changes to the steric and electronic interactions of active site and drug, but rather by cryptic changes to tertiary structure. How selective resistance can be conferred to one drug but not another by a single mutation, for example, the resistance conferred by ^{Hi}V511A to amoxicillin but not ampicillin [53], remains unclear. Proteochemometric modeling used by Nabu *et al*. [55] appears to be a powerful in predicting resistance mutations and other methods seeking to predict the effect of mutations computationally are being developed [73–75]. These, combined with functional enzymology and the vast set of published structure–activity relationship (SAR) data, would provide a unique opportunity to design new inhibitors for these clinically important antibacterial targets. Structural analysis continues to provide critical information toward understanding the mode of antibiotic binding and the emergence of resistance mechanisms.

Supplementary data to this article can be found online at https://doi.org/10.1016/j.jmb.2019.07.010.

Materials and Methods

Chemicals were bought from Sigma-Aldrich® unless otherwise stated. Molecular biology reagents were from New England Biolabs®.

Design, cloning, expression and purification of PBP3 constructs

In this study, PBP3 from *P. aeruginosa* (*Pa*PBP3*) was expressed as a soluble fragment, residues 50–579, lacking the *N*-terminal transmembrane helix, or, to aid crystallographic studies of the active site, only the *C*-terminal transpeptidation (TP) domain were expressed: *E. coli* (*Ec*TP3) (residues 234–588), clinical mutation-mediated penicillin-resistant *N. gonorrhoeae* (*Ng*TP2$^{HR\text{-}6140}$) (residues 237–582) and *H. influenzae* (*Hi*TP3) (residues 254–610). A predicted flexible loop (α9–α10), protruding from the TP domain of all the TP3 constructs, was removed as in the approach followed by Fedarovich *et al*. [30] for the crystallization of the clinical mutant *Ng*PBP2 TP domain (*Ng*TP2$^{t3–6140}$) (see Table 1). The fusion was made through a single glycine at their respective positions: Δ280–294 for *Ec*TP3 and Δ300–314 for *Hi*TP3. *Hi*TP3 could only be crystallized once ITKV (residues 467–470) were mutated to FEKQ (*Hi*TP3^{FEKQ}) (these four residues are on a surface loop located at the antipode of the catalytic pocket). The *N*-terminal leucine in the clinical mutation-mediated penicillin-resistant *Ng*TP2$^{t3–6140}$ construct utilized by Fedarovich *et al*. [30] was mutated to arginine to obtain crystals from novel crystallization conditions diffracting to significantly higher resolutions: *Ng*TP2$^{HR\text{-}6140}$. All constructs were synthesized by Integrated DNA Technologies, except for *Pa*PBP3*, which was amplified from genomic DNA. Constructs were subcloned into pET47b(+) (Novagen) using restriction enzymes *Bam*HI and *Hind*III, except *Pa*PBP3$^{50–579}$ for which *Bam*HI and *Sac*I were utilized. All constructs were expressed and purified with identical protocols: transformed *BL21* (*DE3*) cells were grown in LB media and protein overexpression was carried out at 18 °C for 16 h after induction with 1 mM IPTG, and the *N*-terminal His6-tagged enzymes were purified by reversed Nickel affinity chromatography using recombinant HRV 3C protease for tag cleavage. The protein was subsequently injected onto a 16/60 HiLoad™ Superdex 200 column (GE Healthcare) and eluted in 20 mM Tris–HCl (pH 8) and 400 mM NaCl. Protein-containing fractions were analyzed by SDS-PAGE and the pure fraction combined and concentrated.

Crystallization, data collection and structure solution

All diffraction quality crystals were obtained at 294 K using the hanging drop vapor diffusion method from mixing equal volumes of protein with the following precipitant solutions: 25% (w/v) polyethylene glycol (PEG) 3350, 0.1 M Bis–Tris propane (pH 7.8) and 1% (w/v) protamine sulfate for *Pa*PBP3* at 10 mg/ml (as in Sainsbury *et al*. [33]); 20% PEG 6000, 0.1 M $CaCl_2$, 15% ethylene glycol and 0.1 M Tris–HCl (pH 9) for *Ec*TP3 at 20 mg/ml; 20% PEG 3350 and 0.2 M KNO_3 for *Hi*TP3^{FEKQ} at 25 mg/ml; and 1.0 M sodium citrate, 0.1 M sodium cacodylate (pH 6.5) for *Ng*TP2$^{HR\text{-}6140}$ at 10 mg/ml. Crystals were cryoprotected with 20% glycerol (v/v) prior to flash-freezing in liquid nitrogen. Inhibitor–protein complexes were obtained by soaking crystals overnight with 10 mM compound. Diffraction data were collected on Diamond beamlines I03 and I04. Structures were phased using molecular replacement with MrBump [34]. All data were processed using Dials [35]. Manual building and ligand fitting were performed with COOT [36]. Structures were refined with REFMAC5 [37] and validated with MolProbity [38]. Figures of structures were prepared with PyMOL (The PyMOL Molecular Graphics System, Schrödinger, LLC).

Bocillin fluorescence anisotropy assay

The Bocillin fluorescence anisotropy assay was based on the work of Shapiro [39]. Reactions were performed in 200 μl at ambient temperature (20 °C) in buffer consisting of 100 mM BisTris propane HCl (pH 7.0) and 0.01% Triton X-100 using 96-well black polystyrene assay plates (Greiner). Triton X-100 was included to coat the surface of the plate and prevent adsorption of reagents. The concentration used was below its critical micellar concentration. The assay contained 80 nM protein and was initiated with the addition of 30 nM bocillin. Parallel and perpendicular fluorescence intensities were measured simultaneously at 10 s intervals using a filter-based CLARIOstar plate reader with two emission detectors (BMG Labtech) at λ_{ex} = 482 and λ_{em} = 530 nm. The anisotropy measured is a relative value, not the true anisotropy, because the differential sensitivities of the detectors were not corrected for by the use of a G-factor. Anisotropy was calculated from the parallel and perpendicular fluorescence intensities (I_{para} and I_{perp}, respectively) as follows: Anisotropy = $(I_{para} - I_{perp})/(I_{para} + 2I_{perp})$.

Acknowledgments

The authors would like to acknowledge support from the Newton Fund (MR/P007503/1 and MR/S014934/1), a GCRF Networking Grant (GCRFNG\100347) and a Collaborative Postgraduate award between the University of Warwick and Diamond Light Source (STU0212). *P. aeruginosa* resistant strains were the kind gift of Dr Anders Folkesson, Technical University of Denmark.

Received 4 January 2019;
Received in revised form 2 July 2019;

Accepted 2 July 2019
Available online 10 July 2019

Keywords:
penicillin resistance;
penicillin binding proteins;
PBP3;
crystallography

†These authors have equally contributed to this study.

Abbreviations used:
PG, peptidoglycan; PBP, penicillin-binding protein; HMM, high molecular mass; LMM, low molecular mass; PBD, penicillin-binding domain; GT, glycosyltransferase; TP, transpeptidation; PEG, polyethylene glycol; eg Ec, E.coli; Hi, H. influenzae; Ng, N. gonorrhoeae; Pa, P. aeruginosa.

References

[1] J.M. Frere, M.G. Page, Penicillin-binding proteins: evergreen drug targets, Curr. Opin. Pharmacol. 18 (2014) 112–119.
[2] E. Sauvage, F. Kerff, M. Terrak, J.A. Ayala, P. Charlier, The penicillin-binding proteins: structure and role in peptidoglycan biosynthesis, FEMS Microbiol. Rev. 32 (2008) 234–258.
[3] I. Schweizer, S. Blattner, P. Maurer, K. Peters, D. Vollmer, W. Vollmer, et al., New aspects of the interplay between penicillin binding proteins, murM, and the two-component system CiaRH of penicillin-resistant *Streptococcus pneumoniae* serotype 19A isolates from Hungary, Antimicrob. Agents Chemother. 61 (2017).
[4] K. Bush, P.A. Bradford, β-Lactams and β-lactamase inhibitors: an overview, Cold Spring Harb Perspect Med 6 (2016), a025247. https://doi.org/10.1101/cshperspect.a025247.
[5] J.M. Ghuysen, Serine beta-lactamases and penicillin-binding proteins, Annu. Rev. Microbiol. 45 (1991) 37–67.
[6] E. Sauvage, M. Terrak, Glycosyltransferases and Transpeptidases/Penicillin-Binding Proteins: Valuable Targets for New Antibacterials, Antibiotics (Basel) 5 (1) (2016), 12.
[7] C. Yeats, R.D. Finn, A. Bateman, The PASTA domain: a beta-lactam-binding domain, Trends Biochem. Sci. 27 (2002) 438.
[8] Center for Disease Dynamics EP, State of the World's Antibiotics, CDDEP, Washington, DC, 2015.
[9] K. Bush, A resurgence of β-lactamase inhibitor combinations effective against multidrug-resistant gram-negative pathogens, Int. J. Antimicrob. Agents 46 (2015) 483–493.
[10] S.M. Drawz, K.M. Papp-Wallace, R.A. Bonomo, New β-lactamase inhibitors: a therapeutic renaissance in an MDR world, Antimicrob Agents Chemother (2014) 1835–1846.
[11] D.E. Ehmann, H. Jahić, P.L. Ross, R.F. Gu, J. Hu, G. Kern, et al., Avibactam is a covalent, reversible, non–β-lactam β-lactamase inhibitor, Proceedings of the National Academy of Sciences of the United States of America (2012) 11663–11668.
[12] S.D. Lahiri, S. Mangani, T. Durand-Reville, M. Benvenuti, F. D. Luca, G. Sanyal, et al., Structural Insight into Potent Broad-Spectrum Inhibition with Reversible Recyclization Mechanism: Avibactam in Complex with CTX-M-15 and *Pseudomonas aeruginosa* AmpC β-Lactamases, 2013.
[13] J.M. Munita, C.A. Arias, Mechanisms of antibiotic resistance, Microbiol Spectr. 4 (2016).
[14] M.C. Wissel, D.S. Weiss, Genetic Analysis of the Cell Division Protein FtsI (PBP3): Amino Acid Substitutions that Impair Septal Localization of FtsI and Recruitment of FtsN, 2004.
[15] T.A. Davies, W. Shang, K. Bush, R.K. Flamm, Affinity of doripenem and comparators to penicillin-binding proteins in *Escherichia coli* and *Pseudomonas aeruginosa*, Antimicrob Agents Chemother (2008) 1510–1512.
[16] O. Kocaoglu, E.E. Carlson, Profiling of β-lactam selectivity for penicillin-binding Proteins in *Escherichia coli* strain DC2, Antimicrob Agents Chemother (2015) 2785–2790.
[17] S.M. Markowitz, Isolation of an ampicillin-resistant, non-beta-lactamase-producing strain of *Haemophilus influenzae*, Antimicrob. Agents Chemother. 17 (1980) 80–83.
[18] B.G. Spratt, Hybrid penicillin-binding proteins in penicillin-resistant strains of *Neisseria gonorrhoeae*, Nature. 332 (1988) 173–176.
[19] A. Søndergaard, E.A. Witherden, N. Nørskov-Lauritsen, S.G. Tristram, Interspecies transfer of the penicillin-binding protein 3-encoding gene ftsI between *Haemophilus influenzae* and *Haemophilus haemolyticus* can confer reduced susceptibility to β-lactam antimicrobial agents, Antimicrob. Agents Chemother. 59 (2015) 4339–4342.
[20] E.A. Witherden, M.P. Bajanca-Lavado, S.G. Tristram, A. Nunes, Role of inter-species recombination of the ftsI gene in the dissemination of altered penicillin-binding-protein-3-mediated resistance in *Haemophilus influenzae* and *Haemophilus haemolyticus*, J. Antimicrob. Chemother. 69 (2014) 1501–1509.
[21] C.G. Dowson, A. Hutchison, J.A. Brannigan, R.C. George, D. Hansman, J. Liñares, et al., Horizontal transfer of penicillin-binding protein genes in penicillin-resistant clinical isolates of *Streptococcus pneumoniae*, Proc. Natl. Acad. Sci. U. S. A. 86 (1989) 8842–8846.
[22] C.G. Dowson, A.E. Jephcott, K.R. Gough, B.G. Spratt, Penicillin-binding protein 2 genes of non-β-lactamase-producing, penicillin-resistant strains of *Neisseria gonorrhoeae*, Mol. Microbiol. 3 (1989) 35–41.
[23] T.J. Coffey, M. Daniels, L.K. McDougal, C.G. Dowson, F.C. Tenover, B.G. Spratt, Genetic analysis of clinical isolates of *Streptococcus pneumoniae* with high-level resistance to expanded-spectrum cephalosporins, Antimicrob. Agents Chemother. 39 (1995) 1306–1313.
[24] N. Mouz, A.M. Di Guilmi, E. Gordon, R. Hakenbeck, O. Dideberg, T. Vernet, Mutations in the active site of penicillin-binding protein PBP2x from *Streptococcus pneumoniae* : role in the specificity for β-lactam antibiotics, J. Biol. Chem. 274 (1999) 19175–19180.
[25] D.M. Whiley, N. Goire, S.B. Lambert, S. Ray, E.A. Limnios, M.D. Nissen, et al., Reduced susceptibility to ceftriaxone in *Neisseria gonorrhoeae* is associated with mutations G542S, P551S and P551L in the gonococcal penicillin-binding protein 2, J. Antimicrob. Chemother. 65 (2010) 1615–1618.
[26] ce:other-ref id="or0005">Ubukata K, Shibasaki Y, Yamamoto K, Chiba N, Hasegawa K, Takeuchi Y, et al. Association of amino acid substitutions in penicillin-binding protein 3 with β-lactam resistance in β-lactamase-negative ampicillin-resistant *Haemophilus influenzae*. Antimicrob Agents Chemother 2001. p. 1693–9.
[27] H. Dabernat, C. Delmas, M. Seguy, R. Pelissier, G. Faucon, S. Bennamani, et al., Diversity of beta-lactam resistance-conferring amino acid substitutions in penicillin-binding protein 3 of *Haemophilus influenzae*, Antimicrob. Agents Chemother. 46 (2002) 2208–2218.

[28] S.T. Clark, U. Sinha, Y. Zhang, P.W. Wang, S.L. Donaldson, B. Coburn, et al., Penicillin binding protein 3 is a common adaptive target among *Pseudomonas aeruginosa* isolates from adult cystic fibrosis patients treated with β-lactams, Int. J. Antimicrob. Agents 53 (2019) 620–628.
[29] R.A. Alm, M.R. Johnstone, S.D. Lahiri, Characterization of *Escherichia coli* NDM isolates with decreased susceptibility to aztreonam/avibactam: role of a novel insertion in PBP3, J. Antimicrob. Chemother. 70 (2015) 1420–1428.
[30] A. Fedarovich, E. Cook, J. Tomberg, R.A. Nicholas, C. Davies, Structural effect of the Asp345a insertion in penicillin-binding protein 2 from penicillin-resistant strains of *Neisseria gonorrhoeae*, Biochemistry. 53 (2014) 7596–7603.
[31] A.J. Powell, J. Tomberg, A.M. Deacon, R.A. Nicholas, C. Davies, Crystal structures of penicillin-binding protein 2 from penicillin-susceptible and -resistant strains of *Neisseria gonorrhoeae* reveal an unexpectedly subtle mechanism for antibiotic resistance, J. Biol. Chem. 284 (2009) 1202–1212.
[32] J. Tomberg, A. Fedarovich, L.R. Vincent, A.E. Jerse, M. Unemo, C. Davies, et al., Alanine 501 Mutations in Penicillin-Binding Protein 2 from *Neisseria gonorrhoeae*: Structure, Mechanism, and Effects on Cephalosporin Resistance and Biological Fitness, 2017.
[33] S. Sainsbury, L. Bird, V. Rao, S.M. Shepherd, D.I. Stuart, W.N. Hunter, et al., Crystal structures of penicillin-binding protein 3 from *Pseudomonas aeruginosa*: comparison of native and antibiotic-bound forms, J. Mol. Biol. 405 (2011) 173–184.
[34] R.M. Keegan, M.D. Winn, MrBUMP: an automated pipeline for molecular replacement, Acta Crystallogr. D Biol. Crystallogr. 64 (2008) 119–124.
[35] G. Winter, D.G. Waterman, J.M. Parkhurst, A.S. Brewster, R.J. Gildea, M. Gerstel, et al., DIALS: implementation and evaluation of a new integration package, Acta crystallographica Section D, Structural biology. 74 (2018) 85–97.
[36] P. Emsley, B. Lohkamp, W.G. Scott, K. Cowtan, Features and development of Coot, Acta Crystallogr. D Biol. Crystallogr. 66 (2010) 486–501.
[37] G.N. Murshudov, A.A. Vagin, E.J. Dodson, Refinement of macromolecular structures by the maximum-likelihood method, Acta Crystallogr. D Biol. Crystallogr. 53 (1997) 240–255.
[38] V.B. Chen, W.B. Arendall 3rd, J.J. Headd, D.A. Keedy, R.M. Immormino, G.J. Kapral, et al., MolProbity: all-atom structure validation for macromolecular crystallography, Acta crystallographica Section D. Biological crystallography. 66 (2010) 12–21.
[39] A.B. Shapiro, Investigation of beta-lactam antibacterial drugs, beta-lactamases, and penicillin-binding proteins with fluorescence polarization and anisotropy: a review, Methods and applications in fluorescence. 4 (2016), 024002.
[40] S. Pares, N. Mouz, Y. Pétillot, R. Hakenbeck, O. Dideberg, X-ray structure of *Streptococcus pneumoniae* PBP2x, a primary penicillin target enzyme, Nat. Struct. Biol. 3 (1996) 284–289.
[41] H. Faruki, P.F. Sparling, Genetics of resistance in a non-beta-lactamase-producing gonococcus with relatively high-level penicillin resistance, Antimicrob. Agents Chemother. 30 (1986) 856–860.
[42] E. Sauvage, A. Derouaux, C. Fraipont, M. Joris, R. Herman, M. Rocaboy, et al., Crystal structure of penicillin-binding protein 3 (PBP3) from *Escherichia coli*, PLoS One 9 (2014), e98042.
[43] Y. Chen, W. Zhang, Q. Shi, D. Hesek, M. Lee, S. Mobashery, et al., Crystal structures of penicillin-binding protein 6 from *Escherichia coli*, J. Am. Chem. Soc. 131 (2009) 14345–14354.
[44] P. Macheboeuf, A.M. Di Guilmi, V. Job, T. Vernet, O. Dideberg, A. Dessen, Active site restructuring regulates ligand recognition in class A penicillin-binding proteins, Proc. Natl. Acad. Sci. U. S. A. 102 (2005) 577–582.
[45] K. Hasegawa, R. Kobayashi, E. Takada, A. Ono, N. Chiba, M. Morozumi, et al., High prevalence of type b beta-lactamase-non-producing ampicillin-resistant *Haemophilus influenzae* in meningitis: the situation in Japan where Hib vaccine has not been introduced, J. Antimicrob. Chemother. 57 (2006) 1077–1082.
[46] Y. Osaki, Y. Sanbongi, M. Ishikawa, H. Kataoka, T. Suzuki, K. Maeda, et al., Genetic approach to study the relationship between penicillin-binding protein 3 mutations and *Haemophilus influenzae* β-lactam resistance by using site-directed mutagenesis and gene recombinants, Antimicrob. Agents Chemother. 49 (2005) 2834.
[47] Skaare D, Anthonisen IL, Kahlmeter G, Matuschek E, Natås OB, Steinbakk M, et al. Emergence of clonally related multidrug resistant *Haemophilus influenzae* with penicillin-binding protein 3-mediated resistance to extended-spectrum cephalosporins, Norway, 2006 to 2013. 2014.
[48] Sanbongi Y, Suzuki T, Osaki Y, Senju N, Ida T, Ubukata K. Molecular evolution of β-lactam-resistant *Haemophilus influenzae*: 9-year surveillance of penicillin-binding protein 3 mutations in isolates from Japan. 2006.
[49] J. Tomberg, M. Unemo, C. Davies, R.A. Nicholas, Molecular and structural analysis of mosaic variants of penicillin-binding protein 2 conferring decreased susceptibility to expanded-spectrum cephalosporins in *Neisseria gonorrhoeae*: role of epistatic mutations, Biochemistry. 49 (2010) 8062–8070.
[50] K. Straker, M. Wootton, A.M. Simm, P.M. Bennett, A.P. MacGowan, T.R. Walsh, Cefuroxime resistance in non-beta-lactamase *Haemophilus influenzae* is linked to mutations in ftsI, J. Antimicrob. Chemother. 51 (2003) 523–530.
[51] García-Cobos S, Campos J, Lázaro E, Román F, Cercenado E, García-Rey C, et al. Ampicillin-resistant non-β-lactamase-producing *Haemophilus influenzae* in Spain: recent emergence of clonal isolates with increased resistance to cefotaxime and cefixime. 2007.
[52] A.C. Fluit, A. Florijn, J. Verhoef, D. Milatovic, Susceptibility of European beta-lactamase-positive and -negative *Haemophilus influenzae* isolates from the periods 1997/1998 and 2002/2003, J. Antimicrob. Chemother. 56 (2005) 133–138.
[53] K. Kishii, N. Chiba, M. Morozumi, K. Hamano-Hasegawa, K. Ubukata, I. Kurokawa, et al., Diverse mutations in the ftsI gene in ampicillin-resistant *Haemophilus influenzae* isolates from pediatric patients with acute otitis media, J. Infect. Chemother. 16 (2010) 87–93.
[54] A. Mizoguchi, S. Hitomi, Cefotaxime-non-susceptibility of *Haemophilus influenzae* induced by additional amino acid substitutions of G555E and Y557H in altered penicillin-binding protein 3, J. Infect. Chemother. 25 (2019) 509–513.
[55] S. Nabu, C. Nantasenamat, W. Owasirikul, R. Lawung, C. Isarankura-Na-Ayudhya, M. Lapins, et al., Proteochemometric model for predicting the inhibition of penicillin-binding proteins, J. Comput. Aided Mol. Des. 29 (2015) 127–141.
[56] M. Liao, Vaccine and Infectious Disease Organization UoS, Department of Microbiology and Immunology UoS, W.-M. Gu, Shanghai Skin Disease and STD Hospital WYR, Y. Yang, et al., Analysis of mutations in multiple loci of *Neisseria gonorrhoeae* isolates reveals effects of PIB, PBP2 and MtrR on reduced susceptibility to ceftriaxone, Journal of Antimicrobial Chemotherapy 66 (2018) 1016–1023.
[57] M. Adler, M. Anjum, D.I. Andersson, L. Sandegren, Influence of acquired beta-lactamases on the evolution of spontaneous

carbapenem resistance in *Escherichia coli*, J. Antimicrob. Chemother. 68 (2013) 51–59.
[58] D.M. Whiley, E.A. Limnios, S. Ray, T.P. Sloots, J.W. Tapsall, Diversity of penA alterations and subtypes in *Neisseria gonorrhoeae* strains from Sydney, Australia, that are less susceptible to ceftriaxone, Antimicrob Agents Chemother (2007) 3111–3116.
[59] Tomberg J, Temple B, Fedarovich A, Davies C, Nicholas RA. A highly conserved interaction involving the middle residue of the SXN active-site motif is crucial for function of class B penicillin-binding proteins: mutational and computational analysis of PBP 2 from *N. gonorrhoeae*. 2012.
[60] J.A. Brannigan, I.A. Tirodimos, Q.Y. Zhang, C.G. Dowson, B. G. Spratt, Insertion of an extra amino acid is the main cause of the low affinity of penicillin-binding protein 2 in penicillin-resistant strains of *Neisseria gonorrhoeae*, Mol. Microbiol. 4 (1990) 913–919.
[61] J.A. Kelly, J.R. Knox, H. Zhao, J.M. Frere, J.M. Ghaysen, Crystallographic mapping of beta-lactams bound to a D-alanyl–D-alanine peptidase target enzyme, J. Mol. Biol. 209 (1989) 281–295.
[62] A.R. Barbosa, M. Giufrè, M. Cerquetti, M.P. Bajanca-Lavado, Polymorphism in ftsI gene and β-lactam susceptibility in Portuguese *Haemophilus influenzae* strains: clonal dissemination of β-lactamase-positive isolates with decreased susceptibility to amoxicillin/clavulanic acid, J. Antimicrob. Chemother. 66 (2011) 788–796.
[63] A. Aguirre-Quinonero, I.C. Perez Del Molino, C.G. de la Fuente, M.C. Sanjuan, J. Aguero, L. Martinez-Martinez, Phenotypic detection of clinical isolates of *Haemophilus influenzae* with altered penicillin-binding protein 3, Eur. J. Clin. Microbiol. Infect. Dis. 37 (2018) 1475–1480.
[64] S. Tristram, M.R. Jacobs, P.C. Appelbaum, Antimicrobial Resistance in *Haemophilus influenzae*, 2007.
[65] F.S. Kaczmarek, T.D. Gootz, F. Dib-Hajj, W. Shang, S. Hallowell, M. Cronan, Genetic and molecular characterization of β-lactamase-negative ampicillin-resistant *Haemophilus influenzae* with unusually high resistance to ampicillin, Antimicrob Agents Chemother (2004) 1630–1639.
[66] L. Pernot, L. Chesnel, A. Le Gouellec, J. Croize, T. Vernet, O. Dideberg, et al., A PBP2x from a clinical isolate of *Streptococcus pneumoniae* exhibits an alternative mechanism for reduction of susceptibility to beta-lactam antibiotics, J. Biol. Chem. 279 (2004) 16463–16470.
[67] C. Contreras-Martel, C. Dahout-Gonzalez, S. Martins Ados, M. Kotnik, A. Dessen, PBP active site flexibility as the key mechanism for beta-lactam resistance in pneumococci, J. Mol. Biol. 387 (2009) 899–909.
[68] S.S. van Berkel, J.E. Nettleship, I.K. Leung, J. Brem, H. Choi, D.I. Stuart, et al., Binding of (5S)-penicilloic acid to penicillin binding protein 3, ACS Chem. Biol. 8 (2013) 2112–2116.
[69] J. Thegerström, E. Matuschek, Y.-C. Su, K. Riesbeck, F. Resman, A novel PBP3 substitution in *Haemophilus influenzae* confers reduced aminopenicillin susceptibility, BMC Microbiol. 18 (2018) 48.
[70] Y. Sanbongi, T. Suzuki, Y. Osaki, N. Senju, T. Ida, K. Ubukata, Molecular evolution of beta-lactam-resistant *Haemophilus influenzae*: 9-year surveillance of penicillin-binding protein 3 mutations in isolates from Japan, Antimicrob. Agents Chemother. 50 (2006) 2487–2492.
[71] S. Han, R.P. Zaniewski, E.S. Marr, B.M. Lacey, A.P. Tomaras, A. Evdokimov, et al., Structural basis for effectiveness of siderophore-conjugated monocarbams against clinically relevant strains of *Pseudomonas aeruginosa*, Proc. Natl. Acad. Sci. U. S. A. 107 (2010) 22002–22007.
[72] S. Takahata, N. Senju, Y. Osaki, T. Yoshida, T. Ida, Amino acid substitutions in mosaic penicillin-binding protein 2 associated with reduced susceptibility to cefixime in clinical isolates of *Neisseria gonorrhoeae*, Antimicrob. Agents Chemother. 50 (2006) 3638–3645.
[73] G.M. Verkhivker, Biophysical simulations and structure-based modeling of residue interaction networks in the tumor suppressor proteins reveal functional role of cancer mutation hotspots in molecular communication, Biochimica et Biophysica Acta (BBA)—General Subjects 1863 (2018) 210–225.
[74] R. Farhoodi, M. Shelbourne, R. Hsieh, N. Haspel, B. Hutchinson, F. Jagodzinski, Predicting the effect of point mutations on protein structural stability, Proceedings of the 8th ACM International Conference on Bioinformatics, Computational Biology,and Health Informatics, ACM, Boston, MA 2017, pp. 247–252.
[75] M.J. Latallo, G.A. Cortina, S. Faham, R.K. Nakamoto, P.M. Kasson, Predicting allosteric mutants that increase activity of a major antibiotic resistance enzyme, Chem. Sci. 8 (2017) 6484–6492.
[76] L. Dzhekieva, M. Rocaboy, F. Kerff, P. Charlier, E. Sauvage, R.F. Pratt, Crystal structure of a complex between the actinomadura R39 dd-peptidase and a peptidoglycan-mimetic boronate inhibitor: interpretation of a Transition State Analogue in Terms of Catalytic Mechanism, Biochemistry 49 (30) (2010) 6411–6419, https://doi.org/10.1021/bi100757c.
[77] Y. Zhang, A. Kashikar, C.A. Brown, G. Denys, K. Bush, Unusual escherichia coli PBP 3 insertion sequence identified from a collection of carbapenem-resistant enterobacteriaceae tested *in vitro* with a combination of ceftazidime-, ceftaroline-, or aztreonam-avibactam, Antimicrob. Agents Chemother. 61 (8) (2017) e00389–e003817, https://doi.org/10.1128/AAC.00389-17.